Available online at www.sciencedirect.com

SCIENCE DIRECT®

Ecological Modelling 169 (2003) 131–155

ECOLOGICAL MODELLING

www.elsevier.com/locate/ecolmodel

A remote sensing-based primary production model for grassland biomes

J.W. Seaquist [a,*], L. Olsson [b], J. Ardö [c]

[a] *Department of Geography & Centre for Climate and Global Change Research, McGill University, 805 Sherbrooke St. W., Montreal, Quebec, Canada H3A 2K6*

[b] *Centre for Environmental Studies, Lund University, Box 170, S-221 00 Lund, Sweden*

[c] *Department of Physical Geography and Ecosystems Analysis, Lund University, Box 118, S-221 00 Lund, Sweden*

Received 13 February 2002; received in revised form 17 June 2003; accepted 16 July 2003

Abstract

That data from polar orbiting satellites have detected a widespread increase in photosynthetic activity over the last 20 years in the grasslands of the Sahel is justifies investigating its role in the tropical carbon cycle. But this task is undermined because ground data that are generally used to support the use of primary production models elsewhere are lacking. In this paper, we profile a Light Use Efficiency (LUE) model of primary production parameterised with satellite information, and test it for the West African Sahel; solar radiation is absorbed by plants to provide energy for photosynthesis, while moisture shortfalls control the efficiency of light usage. In particular, we show how an economical use of existing, yet meagre data sets can be used to circumvent nominal, yet untenable approaches for achieving this for the region. Specifically, we use a cloudiness layer provided with the NOAA/NASA 8 km Pathfinder Land data archive (PAL) data set to derive solar radiation (and other energy balance terms) required to implement the model (monthly time-step). Of particular note, we index growth efficiency via transpiration by subsuming rangeland-yield formulations into our model. This is important for partially vegetated landscapes where the fate of rainfall is controlled by relative vegetation cover. We accomplish this by using PAL-derived Normalised Difference Vegetation Index (NDVI) to partition the landscape into fractional vegetation cover. A bare soil evaporation model that feeds into bucket model is then applied, thereafter deriving actual transpiration (quasi-daily time-step). We forgo a formal validation of the model due to problems of spatial scale and data limitations. Instead, we generate maps showing model robustness via Monte Carlo simulation. The precision of our Gross Primary Production (GPP) estimates is acceptable, but falls off rapidly for the northern fringes of the Sahel. We also map the locations where errors in the driving variables are mostly responsible for the bulk of uncertainty in predicted GPP, in this case the water stress factor and the NDVI. Comparisons with an independent model of primary production, CENTURY, are relatively poor, yet favourable comparisons are made with previous primary production estimates found for the region in the literature. A spatially exhaustive evaluation of our GPP map is carried out by regressing randomly sampled observations against integrated NDVI, a method traditionally used to quantify absolute amounts of primary production. Our model can be used to quantify stocks and flows of carbon in grasslands over the recent historical period.

Keywords: Light Use Efficiency; Gross Primary Production; Grasslands; NDVI; Sahel; Carbon cycle

1. Introduction

Net Primary Production (NPP) is an important component of the carbon cycle and a key indicator

* Corresponding author. Tel.: +1-514-398-4347; fax: +1-514-398-7437.
E-mail address: Jonathan.Seaquist@mcgill.ca (J.W. Seaquist).

0304-3800/$ – see front matter © 2003 Elsevier B.V. All rights reserved.
doi:10.1016/S0304-3800(03)00267-9

of ecosystem performance (Lobell et al., 2002). For tracking the recent history of continental-scale vegetation dynamics, the Normalised Difference Vegetation Index (NDVI) derived from reflectance data registered by the 'National Oceanic and Atmospheric Administration' Advanced Very High Resolution Radiometer (NOAA AVHRR) has traditionally been used and regarded as a surrogate measure of primary production (Box et al., 1989). However, recent work shows that this index is only a measure of photosynthetic potential (Runyon et al., 1994). Though the NDVI is a quantitative measure, it only yields estimates of relative vegetation amounts. The NDVI may better be used for parameterising models that may more accurately reflect actual changes in primary production, as well as quantifying its absolute amount. Many sophisticated models of this type are now applied routinely in North American and European contexts for tracing the history of ecosystem dynamics, especially in the context of regional or global carbon budgets (e.g. Ruimy et al., 1996; Veroustraete et al., 1996; Kimball et al., 1997; Goetz et al., 1999; Coops et al., 2001; Lobell et al., 2002; Reeves et al., 2001). But the ground-based data networks that most of these models require to generate reliable estimates of primary production at regional or continental scales are lacking for large parts of the Earth's surface, generally due to a dearth of infrastructure, economic woes, and a sparse population. One such region is the Sahel belt of North Africa. Eklundh and Olsson (2003) flag the Sahel as a hotspot for land cover change. For the period 1982–1999, they identify large areas of strong positive trends in NDVI derived from data from the NOAA AVHRR. These findings suggest that the Sahel may play a significant role in the tropical carbon cycle, and constitute at least part of the missing tropical carbon sink discussed by Schimel et al. (2001). From a humanitarian perspective, this region suffers from frequent drought and famine (Hulme, 1989; Olsson, 1993; Nicholson et al., 1998), both of which are intimately tied to primary production.

2. Objectives

This paper describes and tests a satellite data-driven Light Use Efficiency (LUE) model for mapping primary production and tracing its dynamics over the recent historical period (20 years) for the case of the West African Sahel. Another objective is to assess model performance using Monte Carlo simulations, comparisons with other models, and previous results for the region reported in the literature.

3. The LUE concept with emphasis on previous applications in the Sahel

3.1. LUE concept

NPP represents the net flow of carbon to plants from the atmosphere and defines a balance between gross photosynthesis (GPP—Gross Primary Production) and autotrophic respiration. GPP defines photosynthesis before autotrophic respiration losses, while Net Ecosystem Production is NPP less heterotrophic respiration (Maisongrande et al., 1995; Field et al., 1995; Gower et al., 1999).

The remote sensing-based LUE model is defined as follows, and has evolved from Monteith (1972, 1977):

$$\mathrm{GPP} = \sum_{i=1}^{n} \varepsilon_{\mathrm{p}} \varepsilon (a\mathrm{NDVI} + b)\mathrm{PAR} \quad (1)$$

where GPP is the Gross Primary Production summed over the growing season ($\mathrm{g\,m^{-2}}$), ε_{p} is the maximum biological efficiency of PAR conversion to dry matter ($\mathrm{g\,MJ^{-1}\,m^{-2}}$), ε is the environmental stress scalar, NDVI is the (NIR − RED)/(NIR + RED) (unitless), PAR is the incoming photosynthetically active radiation ($\mathrm{MJ\,m^{-2}}$), and a and b are the regression coefficients.

The NIR and RED refer to unitless reflectances in the near infrared and red portions of the electromagnetic spectrum as measured by the AVHRR sensor mounted on the series of NOAA satellites. The NDVI has often been used as a surrogate measure of primary production (Box et al., 1989), yet recent findings suggest that the NDVI is unsatisfactory for this purpose due to the uncoupling of PAR absorption and plant growth (Runyon et al., 1994). In contrast to the earlier empirical models that related growing season sums of NDVI to geo-referenced samples of above-ground NPP (e.g. Tucker et al., 1985; Prince, 1991a), this approach boasts axiomatic rigour (Prince, 1991b) and has the potential to estimate biomass in absolute terms

across different climatic regimes, site characteristics, and scales, thus eliminating the demand for frequent calibration (Reeves et al., 2001).

PAR encompasses the domain of incoming solar radiation between 0.4 and 0.7 μm, and allows green vegetation to undergo photosynthesis (Hall and Rao, 1994). It varies as a function of solar zenith angle, cloudiness and the concentration of atmospheric constituents (water vapour and aerosols), but over time-scales of 1 day or longer, its contribution to incoming global radiation fluctuates within a narrow range between 45 and 50% (Frouin and Pinker, 1995). Fraction of Photosynthetically Active Radiation (FPAR) denotes the fraction of incident PAR absorbed by plants that is used for photosynthesis and is represented here in terms of NDVI. Sensitivity studies with radiation transfer models indicate the relationship remains robust in the presence of pixel heterogeneity, vegetation clumping, and variations in leaf orientation and optical properties (Goward and Huemmrich, 1992; Begue, 1993; Myneni and Williams, 1994). Good area averages may also be provided given the scale invariance of the relationship. This is the pivotal link that facilitates broad scale primary production mapping using the NDVI from the NOAA AVHRR sensor, since it provides a measure of photosynthetic potential (Goetz and Prince, 1999).

The biological efficiency term has been the focus of much debate. Ambiguity and confusion have arisen because this parameter has been determined using inconsistent methods; it sometimes corresponds to total NPP, and often to above-ground NPP, but rarely to GPP (Gower et al., 1999). It also differs between C_3 and C_4 plants. Sometimes it has been deduced from measurements of global radiation or at other times, the PAR intercepted by a vegetation canopy, instead of APAR (e.g. Gower et al., 1999). Some remotely-sensed based models resort to using a theoretical maximum value, ε_p, predicated on the quantum yield and CO_2-dry-matter-conversion factor, multiplied by stress scalars, ε, that yield GPP after which respiration terms are assessed (e.g. Prince and Goward, 1995; Goetz et al., 1999). Still others determine a bulk efficiency term ($\varepsilon_p\varepsilon$ from Eq. (1)) from the slope of daily integrated CO_2 versus PAR regressions (e.g. Maisongrande et al., 1995), thereafter accounting for respiration terms. Finally, ecophysiological simulation models with non-trivial assumptions regarding plant growth and environment may be used to derive this bulk efficiency term after which remotely sensed data are pulled in to compute primary production (White and Running, 1994; Mougin et al., 1995; Handcock, 2001). Stress factors (lumped as ε in Eq. (1)) that down-regulate the potential growth efficiency, ε_p, may include drought, temperature extremes, pollution, herbivory, insufficient nutrients, disease, etc. (Prince, 1991b) and can vary on timescales from seconds to months. Theoretically derived potential efficiencies range between 1.1 and 8.4 g MJ^{-1}, while plot studies of bulk efficiencies give ranges between 0.42 and 3.8 g MJ^{-1} (Goetz and Prince, 1999).

3.2. Previous applications of the LUE approach in the Sahel

Early applications of the satellite-based LUE model in the Sahel prescribed bulk biological efficiency values from the literature (either a single value, or vegetation-specific values) to estimate areal above-ground NPP or crop yield using remotely sensed data with seemingly acceptable results (e.g. Bartholome, 1990; Cherchali et al., 1995). However, given the considerable heterogeneity of the Sahelian landscape in terms of resource availability, doubt had been cast on an invariant bulk biological efficiency term, even for a given species (Begue et al., 1991; Prince, 1991b; Guerif et al., 1993; Hanan et al., 1995). Rasmussen (1998) tested and rejected the hypothesis of stable bulk biological growth efficiency for the Senegalese Sahel and elucidated some of the fundamental relations between above-ground NPP, NOAA AVHRR NDVI imagery, and the environment, by showing that residual unexplained variance in empirical NDVI–NPP relations could be reduced by including surface temperature and percent tree cover in multivariate regression models. Though it is now evident that the bulk biological growth efficiency is not constant, it may converge on a narrow range of values for particular plant functional types in terms of GPP, but not NPP, due to differences in respiration costs. The underlying tenet of the functional convergence hypothesis maintains that plants have been tuned through natural selection to maximise photosynthetic gain per unit APAR (GPP) by optimising resource allocation in environments with limited resources and high acquisition costs (Goetz and Prince, 1999). This

is the major appeal of the LUE approach for computing GPP using remote sensing (Goetz and Prince, 1999).

4. Test area—West African Sahel

The area covers most of Niger and parts of Mali, Burkina Faso, Benin, Nigeria, the Congo, and Chad (between 11°N and 20°N and 1°W and 18°E) all of which are located in the 'Continental Sahel', a term defined by its recognition as a homogeneous rainfall region (Agnew and Chappell, 1999) (Fig. 1). The climate ranges from arid to semi-arid with a sharp north-south precipitation gradient (Maselli et al., 1992). Mean annual rainfall totals range from less than 100 mm $year^{-1}$ in the north to almost 1000 mm in the south. Annual evapotranspiration far exceeds annual rainfall and ranges from 1800 to 2300 mm (Le Houerou, 1980; Rockström, 1997). The rains begin with the northward migration of the inter-tropical convergence zone in May and subside with its southward retreat around the beginning of October. The north is sparsely vegetated with bush-land dominating, giving way to grassland, savannah, and woody savannah in the far south. The vegetation is adapted to a warm, dry climate, with most grasses using the C_4 photosynthetic pathway, while woody species and some herbs exhibit the C_3 (Le Houerou et al., 1993). Marked annual fluctuations occur in the proportion of the different grass species growing at any one site. Nomadic pastoralism is the dominant land use in the north, giving way to shifting or fallow cultivation rotation in the south. Major crops grown include millet, maize sorghum, and cowpea, all of which are C_4 species (Le Houerou, 1980). The soils are sandy with low organic and nutrient content, while topographical variations are generally less than 500 m within the vegetated zones (Le Houerou, 1980).

5. Data sources and preparation

5.1. NOAA/NASA Pathfinder Land data set

We used daily data from the NOAA/NASA Pathfinder Land data archive (PAL) data set to derive many of the parameters needed for Eq. (1). The PAL has spatial resolution of 8 km and includes layers for solar zenith angle, satellite look and azimuth angles, cloud and quality flags, as well as the original five channels of the NOAA AVHRR sensor (red and near-infrared reflectance, and three thermal) (Table 1). These data come corrected for Rayleigh scattering and ozone absorption, and include post-flight sensor calibration (James and Kalluri, 1994; Smith et al.,

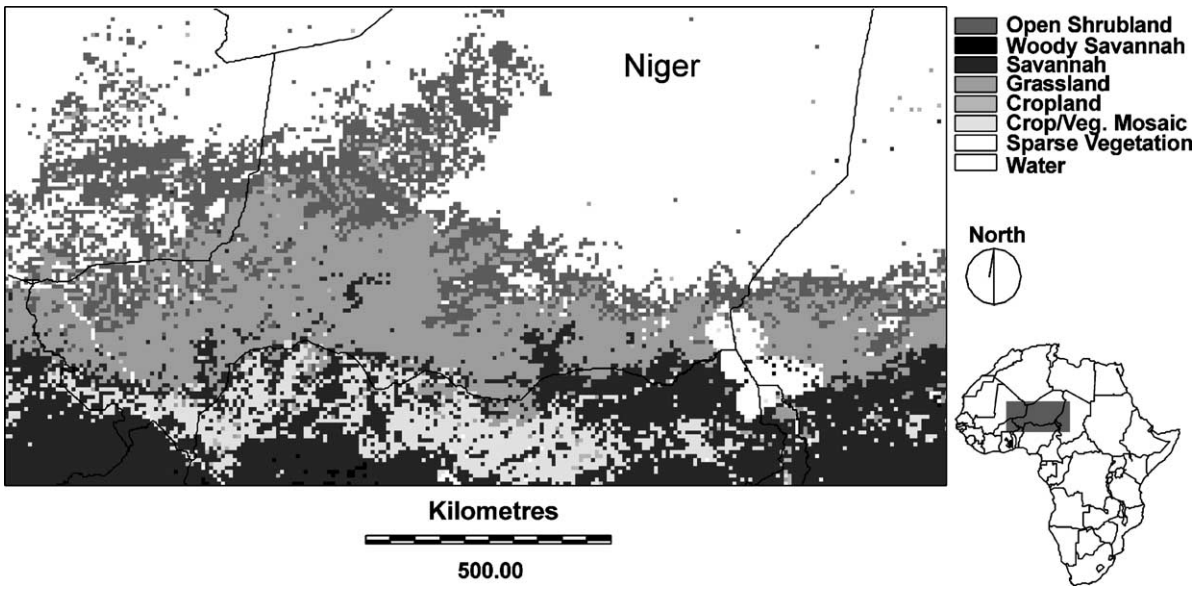

Fig. 1. Map of study area showing International Geosphere Biosphere land cover classes.

Table 1
Data layers provided with the PAL data set

Parameter	Units	Field width	Offset	Gain
NDVI	–	8	128	0.008
CLAVR	–	8	1	1
Quality control flag	–	8	1	1
Scan angle	Radians	16	10481.98	0.0001
Solar zenith angle	Radians	16	10	0.0001
Relative azimuth angle	Radians	16	10	0.0001
Channel 1 reflectance	%	16	10	0.002
Channel 2 reflectance	%	16	10	0.002
Channel 3 brightness temperature	Kelvin	16	−31990	0.005
Channel 4 brightness temperature	Kelvin	16	−31990	0.005
Channel 5 brightness temperature	Kelvin	16	−31990	0.005
Julian day	DDD·HH	16	10	0.01

1997a,b), and is the longest, most consistently processed global satellite imagery archive to date. Known problems include (1) under-estimation of the corrections for Rayleigh and ozone absorption; (2) red and near-infrared channels were not normalised for solar zenith angle, and (3) incorrect computation of the solar zenith angle. Smith et al. (1997a,b) reported these errors affect the NDVI by at most 0.02 NDVI units. The reason for choosing 1992 is the existence of a data set generated by the HAPEX-Sahel (Hydrologic Atmospheric Pilot Experiment in the Sahel—carried out in southwest Niger in 1992) to aid in the construction of our model. The main goal of this international project was to elucidate the mechanisms of land-atmosphere feedback at the scale of a grid cell for a general circulation model ($1^\circ \times 1^\circ$) (Prince et al., 1995).

Maximum value compositing is commonly employed to mitigate unwanted atmospheric and view angle effects in daily NDVI images by 'collapsing' them into mosaics composed of the highest NDVI for each location over a pre-specified time period by sequentially comparing pixels (Holben, 1986). Due to the shortcomings of this method (e.g. Cihlar et al., 1994), we used an alternative approach that selects only those pixels with favourable viewing geometry and minimises bias (Seaquist, 2001). We then filtered then NDVI time profiles using a modified best index slope extraction method (Viovy et al., 1992; Lind and Fensholt, 1999) to rid the images of residual cloud contamination. Finally, we corrected them for the influence of background soil reflectance after Lind and Fensholt (1999).

5.2. Climate data

The climate data were used to derive both energy balance and soil moisture estimates used to compute ε in Eq. (1). We incorporated climate data from four different sources. Mean monthly temperature and monthly rainfall totals were merged from version 1.2 of the Global Historical Climatology Network (Vose et al., 1992) data-base and the Climate Research Unit data-base over the West African Sahel from between 10°N and 20°N to 18°W and 23°E. Both these data sets have undergone extensive screening. The number of rainfall stations for the period May–October was boosted considerably by amalgamating them with 1992 data from Africa Data Dissemination Service. Finally, a minimum and maximum of 79 rainfall stations in November and 257 in June, respectively, were retained (for temperature, 32 in January and 58 in October, respectively). Daily rainfall, and maximum and minimum temperature records for 16 synoptic climate stations across Niger for a 7-year period were provided by the National Meteorological Service in Niamey, Niger.

We generated total monthly rainfall surfaces for June through September of 1992 with universal 'block' kriging (see Matheron, 1971; Goovaerts, 1997; Chappell et al., 2001 for more detailed discussions of this technique) in order to scale up or estimates to match the spatial resolution of the satellite data. Accuracies derived from cross-validation of these variogram models varied between 15 and 20% from June to September. We used thin plate splines

to interpolate rainfall for other months given that (1) there were fewer stations recording rainfall, (2) universal kriging techniques were deemed inappropriate after checking the rainfall distributions (which were highly skewed), and (3) most photosynthesis occurs during the rainy season.

Monthly mean temperatures exhibited smooth and restricted variation. Since there were too few stations to interpolate reliably with kriging, we interpolated using thin plate splines (yielding an root mean square error of 0.7 °C, obtained by leaving HAPEX-Sahel temperature data out of the interpolation procedure).

5.3. Land cover

The Africa Land Cover Characteristics Data-Base version 1.2 with the International Geosphere Biosphere Programme legend provided us with information on land cover (USGS, 2000). This data layer was not used explicitly in our model, but rather to guide our analyses and the interpretation of our results. The data-base was generated at a 1-km spatial resolution, and was derived from AVHRR data acquired between April 1992 and March 1993. The spatial resolution was degraded to 8 km to ensure compatibility with the PAL data set (Fig. 1). The land cover classification has an overall accuracy of 83%, though accuracy was somewhat reduced for the Sahel, with 67% for both shrub-land and savannah (Loveland et al., 1999).

5.4. FAO digital soil map of the world

Since we required information on water holding capacity for the computation of our water stress factor, ε (Eq. (1)), we took the maximum soil moisture storage, computed from topsoil texture and soil depth, from version 3.5 of the Food and Agriculture Organization (FAO) Digital Soil Map of the World (1995) at scale of 1:5,000,000. We recoded the map to obtain estimates of soil moisture storage capacity to an impermeable layer, or to a depth of 100 cm, by taking the centres of the ranges provided in their data-base. For contiguous regions showing a combination of two categories, we applied weighted averaging. The FAO states that the estimation of maximum soil moisture storage was determined in isolation of the prevailing climate and largely ignores the rooting behaviour of vegetation and that the reliability of the soil type classification is questionable for some regions of Africa. This data layer is the only source of information available at this scale.

6. Methods

Fig. 2 illustrates the processing stream. The parameters inside the ellipsoids represent the raw data (including constants derived from the literature) used in the model, whereas the parameters inside the boxes are derived during the execution of the model. Note that Eq. (1) is a highly generalised form of this flowchart, and is depicted in the shaded boxes in Fig. 2. The methods described below are to be reviewed with direct reference to Eq. (1) and Fig. 2.

6.1. PAR

We estimated PAR on cell-by-cell basis to an acceptable level of accuracy (root mean square error of 35.4 $MJ\,m^{-2}\,month^{-1}$) for use with a terrestrial LUE model using the daily CLAVR (CLouds from AVHRR) layer from the PAL data set in combination with Ångström's equation (Fig. 3a). Though Seaquist and Olsson (1999) demonstrate the methodology in detail, we outline the rudiments of this calculation in Appendix A.

6.2. FPAR and APAR

We linearly scaled FPAR between the lower and upper limits of bare soil and maximum NDVI, respectively (NDVI = 0.04, for 0% absorption, and NDVI = 0.61, 95% absorption) (Goward and Huemmrich, 1992; Potter et al., 1993; Guerif et al., 1993; Ruimy et al., 1996; Prince et al., 1995; Hanan et al., 1995; Goetz et al., 1999; Lind and Fensholt, 1999; Handcock, 2001):

$$\mathrm{FPAR} = 1.67(\mathrm{NDVI}) - 0.07 \quad (2)$$

Note that Eq. (2) is the term inside the parentheses in Eq. (1). An NDVI value of 0.04 was determined for bare soil by taking its mean during the dry season, while 0.61 corresponds to a growing season NDVI along the shore of Lake Chad where vegetation is very dense. Finally, we merged the images into monthly means to further reduce noise (Eklundh, 1996;

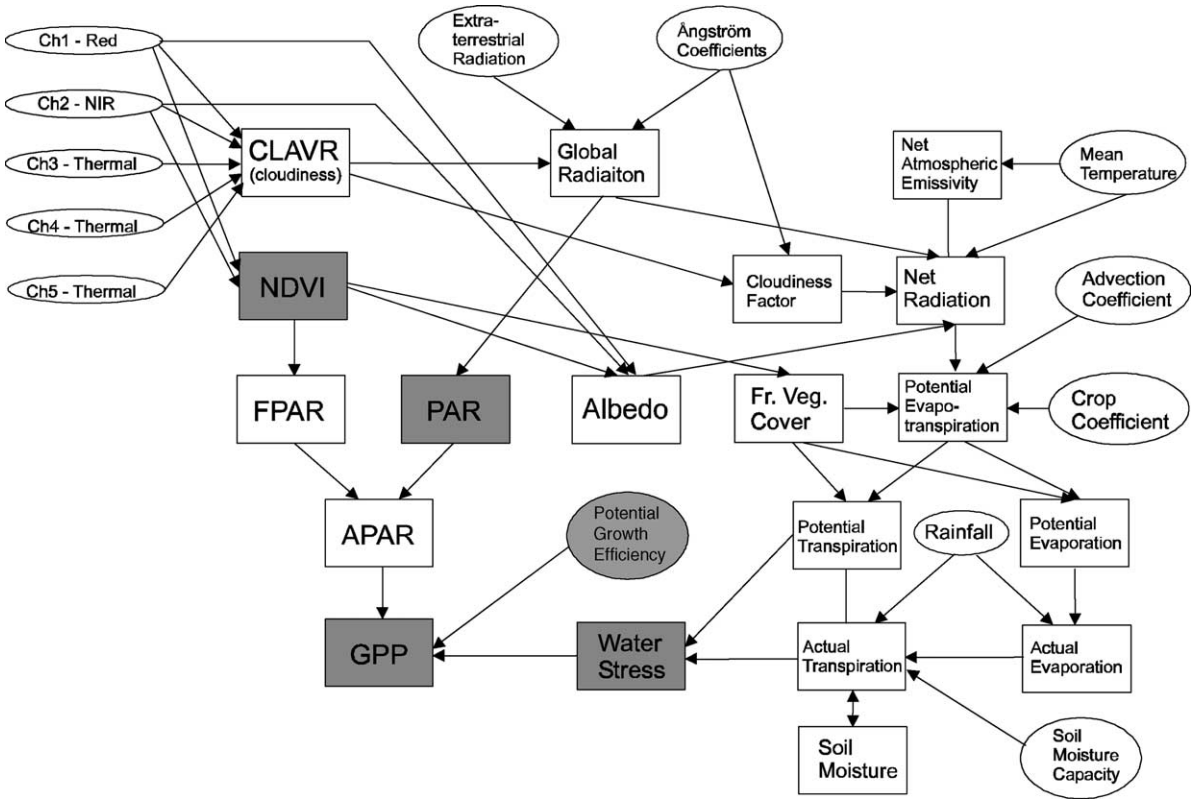

Fig. 2. Flowchart of LUE model.

Kaisischke and French, 1997) thereafter computing APAR as the product of PAR and FPAR for each month (Fig. 3b).

6.3. Potential biological growth efficiency—ε_p

We assigned a value of $5\,g\,MJ^{-1}$ for ε_p (the potential biological efficiency), which indicates a mixture of C_3 and C_4 plants with the assumption that for the greater part of a growing season, C_4 grasses dominate the NOAA AVHRR reflectance signal. Typical Sahelian rangeland consists of a mixture of both C_3 and C_4 plants, with C_3 forbs dominating early in the growing season, giving way to C_4 grasses later in the growing season (Hanan et al., 1995, 1997), at least for typical sites in the HAPEX-Sahel and in the Gourma region of Mali. Mougin et al. (1995) found the C_3/C_4 ratio to be 43/57 for Mali's Ferlo district. The Global Production Efficiency Model of Prince and Goward (1995) and Goetz et al. (1999) uses a value of $6.1\,g\,MJ^{-1}$ for C_4 plants (invariant with temperature), while they model C_3 values based on leaf biochemical processes. The potential efficiency of C_3 plants is generally lower, especially for the higher temperatures of Sahelian environments. Without regarding Prince and Goward's (1995) C_3 potential efficiency sub-routine, all other models, irrespective of complexity, resort to prescribing these values, or conduct error minimisation exercises with actual biomass measurements or use regressions of PAR against CO_2 fluxes (e.g. Potter et al., 1993; Mougin et al., 1995; Ruimy et al., 1996).

6.4. Water stress scalar—ε

Water is generally assumed is the primary factor limiting photosynthesis in the region at these scales (Le Houerou, 1980; Verstraete and Pinty, 1991). We therefore reformulated the equations in Wight and Hanks (1981) and Millington et al. (1994), replacing

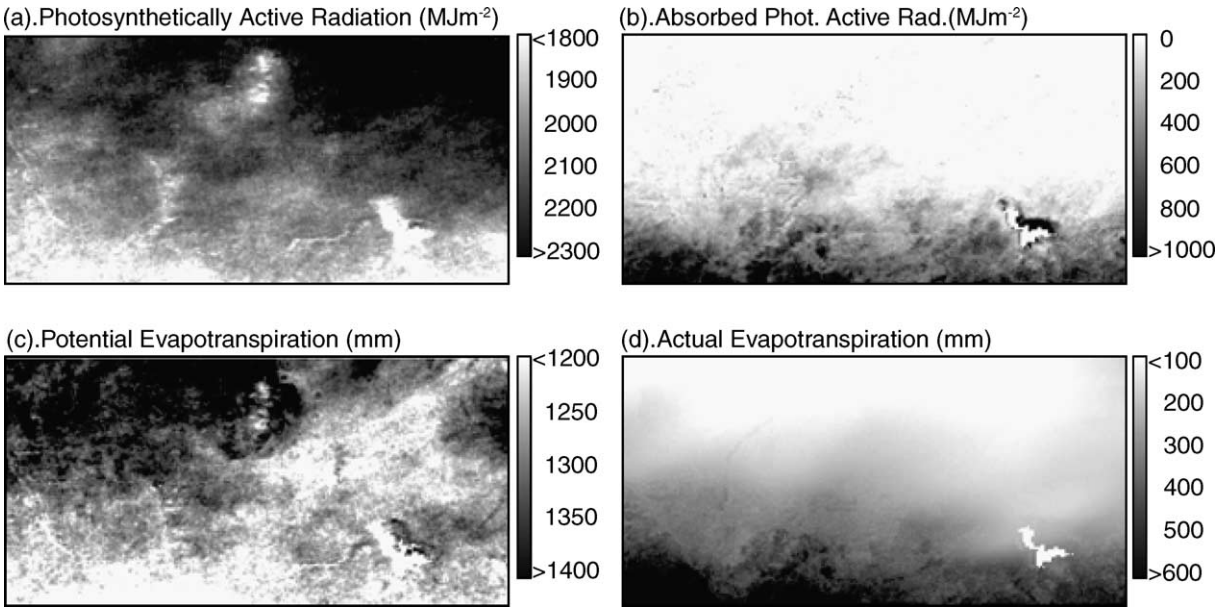

Fig. 3. (a) Total photosynthetically active radiation for the growing season (May–October). (b) Total photosynthetically active radiation absorbed by plant canopy for the growing season. (c) Total potential evapotranspiration for the growing season. (d) Total actual evapotranspiration for the growing season.

their crop yield terms with GPP

$$\frac{\mathrm{GPP_a}}{\mathrm{GPP_p}} = \frac{T_a}{T_p} \tag{3}$$

where $\mathrm{GPP_a}$ is the Gross Primary Production ($\mathrm{g\,m^{-2}}$), $\mathrm{GPP_p}$ is the potential Gross Primary Production ($\mathrm{g\,m^{-2}}$), T_a is the actual transpiration (mm), and T_p is the potential transpiration.

The ratio of actual transpiration to potential transpiration is the water stress scalar. Note that in terms of Eq. (1), $\mathrm{GPP_p}$ is directly analogous to the product of the growing season sum of APAR and the potential biological efficiency, ε_p. The purpose of Eq. (3) is to provide a logical argument and point of departure for our derivation of water stress, ε. The calculation of potential transpiration is discussed first, followed by actual transpiration.

A realistic assessment of actual transpiration (as well as actual evapotranspiration) from partially vegetated surfaces requires, as a minimum, the separate treatment of bare soil and plant components (Hanks, 1974; Wight and Hanks, 1981; Wallace et al., 1993; Millington et al., 1994; Mougin et al., 1995; Srivastava et al., 1997). We therefore partitioned our estimate of potential evapotranspiration (see derivation below) into bare soil and vegetation components by transforming the NDVI into fraction of vegetation cover ranging from 0 (no vegetation cover) and 1 (full vegetation cover). We followed Choudhury (1994), Capehart (1996), and Carlson and Ripley (1997):

$$E_p = K_c ET_p \left[1 - \left(\frac{\mathrm{NDVI} - \mathrm{NDVI_o}}{\mathrm{NDVI_s} - \mathrm{NDVI_o}}\right)^2\right] \tag{4}$$

$$T_p = K_c ET_p \left(\frac{\mathrm{NDVI} - \mathrm{NDVI_o}}{\mathrm{NDVI_s} - \mathrm{NDVI_o}}\right)^2 \tag{5}$$

where E_p is the bare soil potential evaporation (mm), T_p is the potential transpiration (mm), K_c is the crop coefficient, ET_p is the potential evapotranspiration (mm), NDVI is the cell-specific NDVI, $\mathrm{NDVI_s}$ is the NDVI corresponding to full vegetation cover (0.50), and $\mathrm{NDVI_o}$ is the bare soil NDVI (0.04).

The logic behind Eqs. (4) and (5) are outlined in Appendix B. We assigned a constant value of 0.85 in accordance with typical mean growing season values for rangeland vegetation (Wight and Hanks, 1981; Millington et al., 1994). We used the Priestley and Taylor (1972) method for computing potential

evapotranspiration (Fig. 3c) for Eqs. (4) and (5) because of its direct physical link with radiation, its success in operational agro-meteorological monitoring, data availability, as well as its suitability for large areas (Bastiaanssen, 1995; Jiang and Islam, 1999):

$$ET_p = \alpha_a \frac{\Delta}{\Delta + \gamma}(R_n - G) \quad (6)$$

where α_a is the advection parameter, Δ is the gradient of saturated vapour pressure (kPa $^\circ C^{-1}$), γ is the psychrometric constant (kPa $^\circ C^{-1}$), R_n is the net radiation (MJ m^{-2}), and G is the ground heat flux (MJ m^{-2}).

The ground heat flux is considered negligible and is ignored. Most measurements in humid, temperate environments have shown that the advection parameter takes on a conservative value of about 1.3, though in arid environments, values in excess of 1.75 are reported (Jensen et al., 1990), likely due to the entrainment of heat from both above and below, leading to a significant increase in the depth of the planetary boundary layer (Monteith and Unsworth, 1990; L'homme, 1996). We selected a value of 1.46 (based on monthly sums) as this number optimised the agreement between estimated and measured potential evapotranspiration giving an root mean square error of 16.3 mm against ground data from the HAPEX-Sahel experimental site at a monthly time step. Appendix C outlines the computation of net radiation in Eq. (6).

We then calculated the actual transpiration (see Eq. (3)) with a simple bucket model where the root zone is given as a single layer with a constant water holding capacity where:

$$T_{a(t)} = SM_{(t)} + R_{(t)} - E_{a(t)} - SM_{(t+1)} - D_{(t)} \quad (7)$$

where t is the day, SM is the soil moisture (mm), R is the rainfall (mm), E_a is the actual evaporation from bare soil (mm), T is the transpiration (mm), D is the drainage and runoff (mm).

The derivation of bare soil actual evaporation from Eq. (7) is given in Appendix D. Deep drainage, runoff, and run-on, are usually infrequent in semi-arid environments (Le Houerou, 1980; Lo Seen Chong et al., 1993; Mougin et al., 1995; Wythers et al., 1999) these were ignored. Water discharge in the Niger River confirms the miniscule contribution of drainage and runoff (Nicholson et al., 1996). The primary function of the bucket model is to parameterise the effect of low soil moisture on the stomatal conductance of vegetation, giving a measure of the impact of drought stress on plant growth:

$$T_a = T_p, \quad \text{if } \frac{SM}{SM_{max}} \geq C \quad (8)$$

$$T_a = \frac{T_p}{C}\frac{SM}{SM_{max}}, \quad \text{if } \frac{SM}{SM_{max}} < C \quad (9)$$

T_a is the actual transpiration (mm), T_p is the potential transpiration (mm), SM is same as defined previously, SM_{max} is the maximum soil water holding capacity (mm), and C is the critical fraction of available water below which soil water deficit affects transpiration.

In reality, the C parameter varies with vegetation and crop type, and can range between 0.28 and 0.7 (Wight and Hanks, 1981; Choudhury and DiGirolamo, 1998). However, both Wight and Hanks (1981) and Millington et al. (1994) used a value of unity (linear relationship) justified on (1) model insensitivity to values below 0.4, (2) the satisfactory performance for rangeland vegetation in both North America and Tunisia, and (3) the lack of information about these data. We assigned a value of 1. We spun up the bucket model by duplicating all pseudo-daily data for 1992 four times (for a time-series of 4 years) to ensure that our estimates achieved independence from arbitrarily assigned initial soil moisture content.

Fig. 3d shows total growing season actual evapotranspiration over the region. Our experiments that tested the sensitivity of actual evapotranspiration to ±20% variations in selected model soil texture parameters (see Appendix D) as well as potential evapotranspiration (corresponding to an area located in the East Central Supersite of the HAPEX-Sahel) revealed that it was most sensitive to rainfall. Observed actual evapotranspiration over a millet field (13°33′N and 2°39′E) in August, and over a herb site (13°33′N and 2°41′E) in both August and September in the South Central Supersite of the HAPEX-Sahel nevertheless confirmed the realistic performance of the model (with the tendency to slightly overestimate actual evapotranspiration).

7. Results

Fig. 4a shows the final map of total growing season GPP (May–October). GPP is very low in the northern

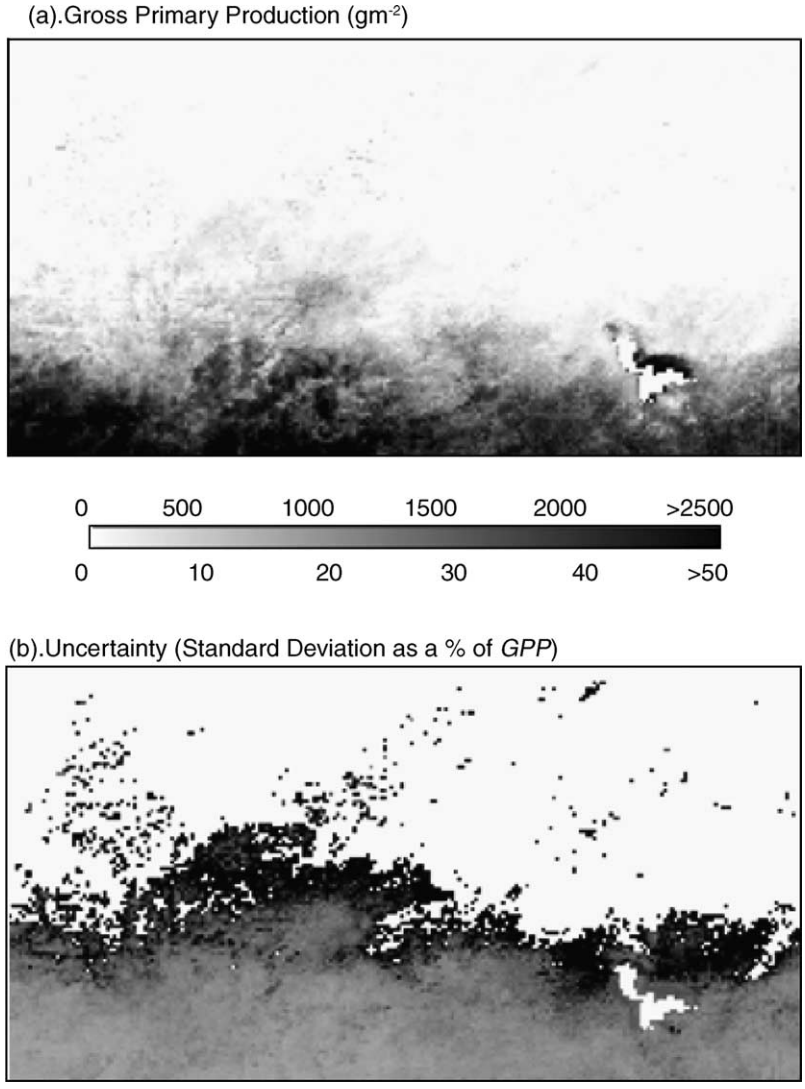

Fig. 4. (a) Growing season GPP for 1992. (b) Standard deviation expressed as a percentage of 1992 growing season GPP as calculated from a Monte Carlo simulation; number of runs = 1000.

regions where it is too dry to support extensive plant communities. Local vegetation pockets are apparent in the mountains north of Agadez where elevations in are in excess of 2000 m. Other patches of GPP are assumed to occur around wadis. In these regions, GPP is generally less than 100 g m^{-2}, though locally, this may exceed 400 g m^{-2}. The region of contiguous GPP begins just north of Lake Chad in the east and roughly extends in a line north-westward to the middle part of the area, before retreating south-westward. The northerly portion of this belt is the pastoral zone supporting fodder for herds of domesticated sheep, goats and cattle during the rainy season. GPP values here are generally between 100 and 500 g m^{-2}. This roughly corresponds to 'Grassland' in Fig. 1. Immediately to the south of this belt is found the mixed Cropland-vegetation Mosaic where fields of millet and sorghum (with other crops) are interspersed with fallow, containing indigenous grassland and savannah species. GPP here ranges from between 500 and 1500 g m^{-2}. Further south, GPP in excess of 1500 g m^{-2} shows the lush vegetation communities of the savannah and woody savannah

Table 2
Amount and proportion of primary production per land cover class

Land cover	% Area	GPP (Tg)	% GPP_{total}	GPP_{mean} ($g\,m^{-2}$)	GPP_{std}	NPP_{mean} ($g\,m^{-2}$)	Above-ground NPP_{mean} ($g\,m^{-2}$)
Barren/sparse	43.9	15.9	1.7	19.5	123.5	9.4	3.7
Shrubland	13.1	9.0	1.0	37.1	69.2	17.8	7.1
Grassland	18.3	120.1	13.1	352.8	298.2	169.3	67.7
Savannah	17.8	578.4	62.9	1752.7	733.2	841.3	336.5
Cropland-vegetation	6.3	185.8	20.1	1596.5	382.5	766.3	306.5
Cropland	0.3	4.5	0.5	920.9	817.6	442.0	176.8
Woody savannah	0.1	6.2	0.7	2831.8	490.5	1359.3	543.7
Water	0.2	0.0	0.0	0.0	0.0	0.0	0.0
Summary	100.0	919.9	100.0	497.2	796.7	238.7	90.6

zones. Highest GPP is found around the northeast shores of Lake Chad (in excess of $3500\,g\,m^{-2}$) where the high water table supports rich thickets of riparian vegetation.

We disaggregated our GPP estimates on the basis of land cover class (Table 2). Class totals of GPP are given, as well as their means per category, as well as their standard deviations. Despite the spatial extent of the Barren/Sparsely vegetated category (comprising 42.9% of the total area), it supports less than 2% of the region's GPP. Conversely, the savannah class covers only 17.6% of the area, yet supports 63% of the region's photosynthetic gain.

8. Evaluation

We used four techniques to assess model performance: (1) Monte Carlo simulations, (2) comparison with the results of a CENTURY model run, (3) qualitative comparisons with other studies conducted in the West African Sahel, and (4) evaluation against the classical integrated NDVI approach for mapping primary production. Direct comparison with ground estimates of NPP were impossible partly due to lack of data, as well as the difficulties in reconciling the differences in spatial resolution between our results (8 km) and ground samples (typically representative of a few metres at most).

8.1. Monte Carlo simulations

Monte Carlo simulation is a powerful and flexible error propagation technique. The driving parameters of a model are varied randomly N times according to their probability distributions. Each realisation is stored and then used to compute a mean and variance for each cell (e.g. Burrough and McDonnell, 1998; Heuvelink, 1998; Crosetto et al., 2001). In the context of Eq. (1), we define the following:

$$\overline{\mathrm{GPP}}_u = \frac{1}{N}\sum_{i=1}^{N}\mathrm{GPP}_i \tag{10}$$

$$\mathrm{GPPs}_u^2 = \frac{1}{N-1}\sum_{i=1}^{N}(\mathrm{GPP}_i - \overline{\mathrm{GPP}}_u)^2 \tag{11}$$

where $\overline{\mathrm{GPP}}_u$ is the mean GPP computed from u model parameters, N is the number of simulations, GPP_i is the simulation-specific (i) GPP, GPPs_u^2 is the GPP variance computed from u model parameters.

We perturbed the parameters of Eq. (1) as in Table 3 for $N = 1000$ runs per variable. All errors except the NDVI are assumed to be stationary, and originate from normal distributions. We deliberately restricted our Monte Carlo simulations to four lumped input parameters due to the technique's heavy computational demands.

Table 3
Errors used for the Monte Carlo simulations

Input parameter	Root mean square error	Determination of error	Rank
$NDVI_{min}$	0.01 (unitless)	Literature	3
$NDVI_{max}$	0.05 (unitless)	Literature	3
PAR	35.0 ($MJ\,m^{-2}\,month^{-1}$)	Ground measurements	4
ε	0.2 (unitless)	'Expert opinion'	1
ε_p	$g\,MJ\,m^{-2}\,month^{-1}$	Literature	2

We established NDVI uncertainty from Kaufman and Tanre (1996) who randomly select actual aerosol and water vapour optical thickness observations from the Senegalese Sahel (Soufflet et al., 1991) to simulate top-of-the-atmosphere NDVI over a time-invariant ground cover of fescue grass, assuming randomly distributed cloud covers of 50%. Compositing for 9- and 27-day periods yielded NDVI values of 0.61 ± 0.046 and 0.65 ± 0.027, respectively. The variations about the mean result from residual atmospheric contamination, cloud, and scan angle effects. Since the compositing period used in this study is about 14 days, we chose a value of ± 0.05 to represent the uncertainty around the maximum NDVI (0.61). We set bare soil NDVI uncertainty at ± 0.01 (0.04). The absolute value of the NDVI is not of primary interest here; rather, we were interested in the stability of the anchor points defining the FPAR–NDVI relation. Quantisation artefacts may potentially contribute precision uncertainties of similar magnitude (depending on target brightness and solar zenith angle), so our uncertainty estimates represent a 'best-case' scenario. The primary impact of varying the NDVI is to alter the a and b parameters in the FPAR–NDVI relation (Eq. (2)), which is effectively equal to incorrectly identifying the NDVI values that correspond to 95 and 0% PAR absorption. We determined the root mean square error for PAR directly from Seaquist and Olsson (1999), briefly reviewed in Appendix A. We found it impossible to quantitatively determine a root mean square error for the water stress term (ε) due to lack of data. We expect error contributions from the simplified assumptions used for the rainfall and hydrology as well as the inaccuracies in maximum soil water holding capacity, SM_{max}, and therefore set it to ± 0.2 (unitless). Finally, we assumed error for the potential biological efficiency, ε_p, to be $\pm 1.0\,g\,MJ^{-1}$. We determined this from the literature while keeping in mind that the vegetation consists of a blend of C_3 and C_4 species in geographically varying proportions. The influence of mineral nutrition remained unknown.

The results are presented in Fig. 4b. As a general rule, the higher the GPP the more robust the prediction; standard deviations are less than 20% of total GPP up to GPP values of about $1000\,g\,m^{-2}$. Standard deviations inflate to between 25 and 99% of GPP for the southern and northern portions of the grassland land cover class, respectively. We decomposed the total error variance into the proportion of error variance contributed per model parameter (Fig. 5a–d). The PAR term lends the least error, generally less than 15% and decreases moving northward. The NDVI is relatively unimportant for determining the GPP of savannah and Cropland-vegetation Mosaic, but contributes over 90% of the total error variance in the northern portions of the grassland class. The potential biological growth efficiency, ε_p, rarely exceeds 30% of the total error variance, while the model is most sensitive to the water stress scalar, ε.

8.2. The CENTURY model

The Monte Carlo simulation technique cannot report bias. Independent estimates of primary production may be obtained from other models, such as CENTURY. CENTURY is a 'lumped parameter', ecosystem model that can simulate biogeochemical fluxes of carbon, nitrogen, phosphorous, and sulphur, as well as primary production and water balance at a monthly time step (Parton et al., 1987, 1988; Cole et al., 1989; Metherell et al., 1993). The driving variables are monthly precipitation and monthly average minimum and maximum temperature. Soil texture, litter nitrogen, lignin content, and tillage disturbance are also important soil process rate controls. The model has been widely used and validated (Burke et al., 1989; Parton et al., 1993, 1994, 1996; Bromberg et al., 1996; Smith et al., 1997a,b; Mikhailova et al., 2000). The effects of fire, fertilisation, irrigation, grazing, various cultivation and harvest methods, etc. are possible to incorporate in the simulations.

We prescribed land cover type from Fig. 1 which we also used to determine land management characteristics (including fire frequencies, grazing characteristics, and fallow periods) for 16 sites across Niger (Fig. 6a) where data were available to run the model. Table 4 shows the scenarios for the different land cover classes. We derived soil texture from the Soil Map of the World (FAO/UNESCO, 1995). Initial amounts of soil carbon and nitrogen were established by running the model to equilibrium using long-term climate averages. Only 7 years of climate data were available for each station, so 3 years were randomly chosen and duplicated to bring the total up to 10 years, the minimum amount of time necessary to generate long-term climate estimates. No nitrogen fixation

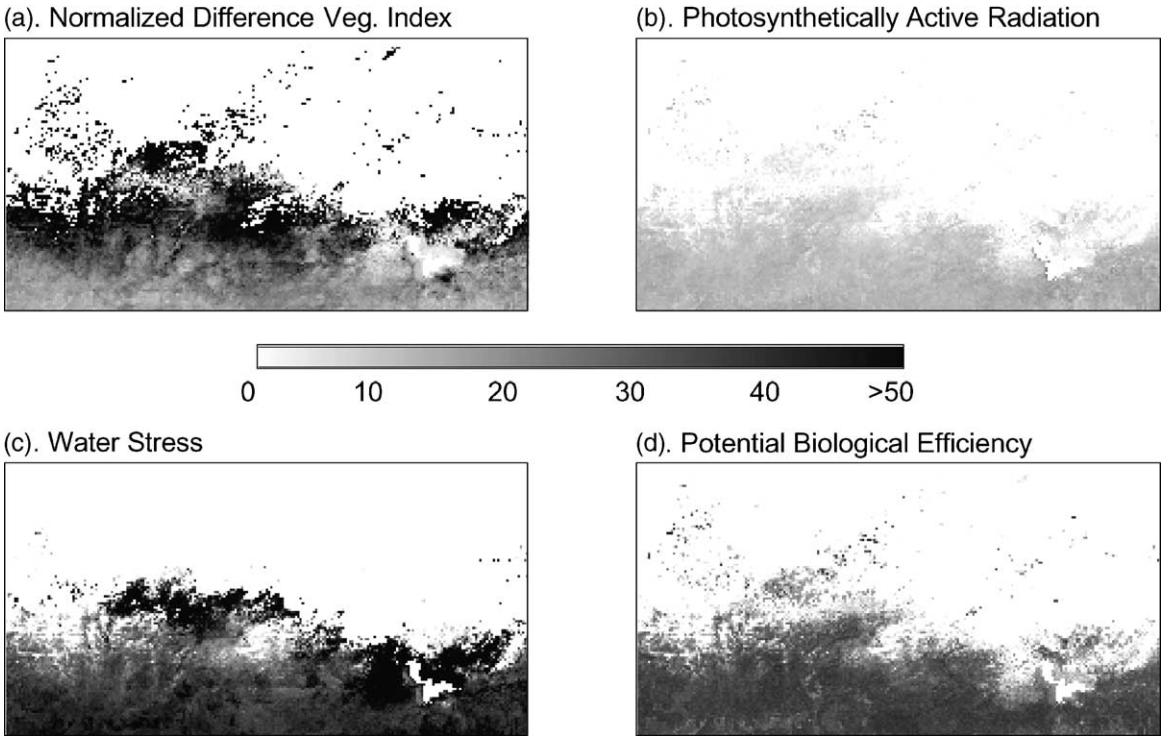

Fig. 5. Percent of total error variance contributed by (a) NDVI, (b) PAR, (c) soil water stress scalar (ε), (d) potential growth efficiency (ε_p).

for *Acacia senegal* was assumed. CENTURY resolves NPP only, and in terms of carbon content. To facilitate comparison with the with our LUE model, we assumed a value of 0.45 for the carbon:dry plant matter ratio, while maintenance and growth respiration were assumed to be 0.64 and 0.75 of GPP, respectively (Hunt, 1994; Prince and Goward, 1995; Handcock, 2001).

Fig. 6b and c show the relationship between CENTURY and PAL GPP. The error bars correspond to the uncertainties computed in PAL GPP from the Monte Carlo simulation. CENTURY generally underestimated the north-south gradient in GPP with an $r = 0.71$. The relationship between equilibrium GPP from CENTURY and PAL GPP (1992) is slightly worse with $r = 0.67$.

Table 4
Scenarios defined for CENTURY runs

Land cover	Grazing	Fire frequency	Agriculture	Pathway	Pre-1992
Sparse	Low intensity (July–October)	No	No	C_4	ditto
Shrubland	Low intensity (July–October)	February every 9th year	No	C_4	ditto
Grassland	Intense (July–September)	February every 5th year	No	C_4	Lower grazing intensity up to 1950
Cropland	Intense after autumn harvest (November–December)	May every year during cropping periods	Rotational millet/ sorghum, no fallow, planting in June	C_4	Fire in February every 9th year up to 1891; decreasing fallow up to 1974; no trees in fallow after 1950
Savannah	Intense (July–October)	February every 5th year	No	C_4	Low intensity grazing up to 1970

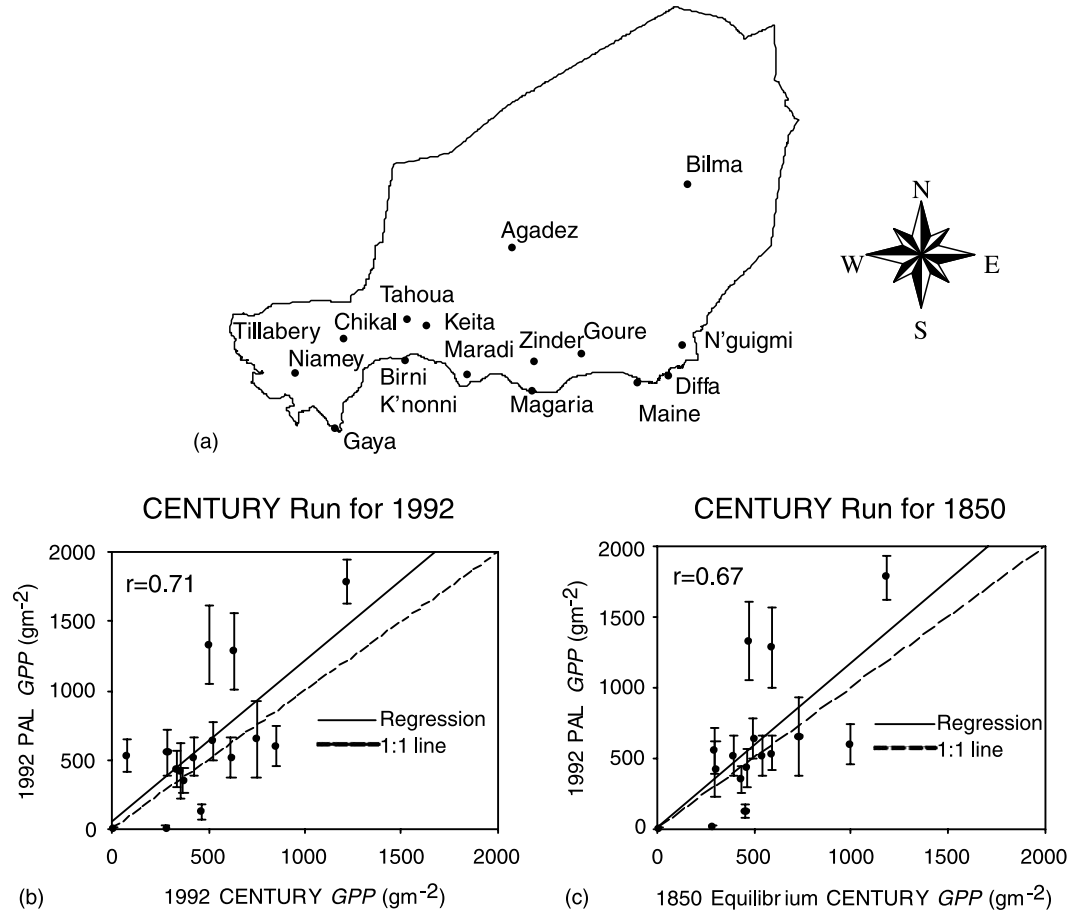

Fig. 6. (a) Sixteen sites across Niger used to parameterise CENTURY. (b) Relationship between 1992 LUE GPP and 1992 CENTURY GPP. (c) Relationship between 1992 LUE GPP and 1850 CENTURY GPP.

There may be multiple reasons for the relatively poor comparison ranging from scale mismatch (point versus pixel) to inaccuracies in the driving variables, to fundamental differences in model assumptions, to the treatment of the respiration terms. CENTURY is a prognostic model whereas the satellite-based method is essentially diagnostic. A major uncertainty in the CENTURY run was the land use management and land use history parameters that, to some extent, determine 1992 GPP. No detailed data were available for these sites, so the scenarios were authorised based on generic knowledge of these patterns in the Sahel (e.g. Ardö and Olsson, 2002). Furthermore, the CENTURY model is more detailed especially in its biogeochemical treatment of primary production, and may be partly identifying biomass reductions due to fertility stress. Finally, most evaluations of CENUTRY have been used to compare the temporal evolution of biomass at one site (with exceptions being the steppes of Russia) (e.g. Parton et al., 1993), whereas the spatial distribution of biomass at one time from several sites were of interest here.

8.3. Qualitative comparison with previous studies

Table 5 gives a summary of the comparisons, which we based on a literature survey. The methods used to predict above-ground NPP in previous studies range from simple above-ground NPP–NDVI correlations, to complex ecophysiological simulation models, and cover a number of scales from point to regional. Qualitative agreement with our LUE model is fair to good.

Table 5
Previous estimates of primary production from the literature compared with estimates from the current LUE model

Location and land use	Year (number of ground samples, correlation coefficient)	Method	Above-ground NPP maps	Above-ground $NPP_{literature}$ ($g\,m^{-2}$)	Above-ground NPP_{LUE} ($g\,m^{-2}$)	Comments	Source
W.A. (cropland)	1984 (n = n/a, r = n/a)	AVHRR LUE Assigned ε_f = 1.5	No	129.5 (mean) <5.8 to >550.0	290.1 0–560.0 (mostly Nigeria)	Crop yields converted with grain:straw ratio of 0.43, used national yield statistics	Bartholome (1990)
WCSS and ECSS HAPEX, S.W. Niger (various)	1992 (n = n/a, r = n/a)	AVHRR LUE Assigned ε_f = 0.5–2.7	No	128.0–144.7	130.2–201.5	Spectral decomposition of pixels, assigned ε based on species	Cherchali et al. (1995)
Maradi, Niger (cropland)	1982–1990 (n = n/a, r = 0.68)	Integrated AVHRR NDVI, empirical	No	93.6–300.0	248.9	Produced time series from ground NPP observations from W.A. (1984–1988)	Prince et al. (1998)
W.A. (grassland)	1984–1988 (n = 172, r = 0.89)	Integrated AVHRR NDVI, empirical	No	0.0–300.0	0.0–435.6	Used NPP ground data sets from Senegal, Mali, Niger	Prince (1991b)
Niger (grassland)	1986–1988 (n = 21–30, r = 0.82–0.95)	Integrated AVHRR NDVI, empirical	No	3.0–280.0	0.0–435.6	Used detailed ground sampling scheme	Wylie et al. (1991)
Senegal (all)	1987–1988 (n = 17–27, r = 0.81–0.90)	Integrated AVHRR NDVI, empirical	Yes	<50.0 to >500.0	0.0 to >600.0	Tree NPP estimates included in regressions	Diallo et al. (1991)
Ferlo, Senegal and Gourma, Mali (grassland)	1976–1987 (n = 127, r = 0.95)	Complex model	Yes	<50.0 to >120.0	0.0–435.6	Used 'mechanistic' ecophysiological simulation model	Mougin et al. (1995)
WCSS HAPEX, Niger (various)	1992 (n = 7–28, r = 0.5–0.91)	LUE + CO_2 supply model	No	60.0—shrubs, 300.0—herb, 120.0—millet	130.2–201.5	Used ground measurements, and favourably compared two plot-based models—results for LUE only given here	Hanan et al. (1995)
Niger + Nigeria (various)	1993 (n = 78, r = 0.84)	Integrated AVHRR NDVI, empirical	Yes	<50.0 to >500.0	0.0 to >600	AVHRR data do not coincide with ground measurements, produced potential NPP for all of Africa	Lo Seen Chong et al. (1993)
Maradi, Niger (cropland)	1983 (n = 6 climate stations, r = 0.75)	Maximum NDVI combined with simple biomass model	No	134.1	248.9	Assumed moisture access only limits plant growth	Justice and Hiernaux (1986)
Senegal (all)	1990–1991 (n = 52, r = 0.91)	Integrated AVHRR NDVI, empirical	Yes	<50.0 to >500.0	0.0 to >600.0	Used NDVI, surface brightness temperature and % tree cover in a multiple regression model with NPP	Rasmussen (1998)
B.F. (grassland)	1987 (n = n/a, r = n/a)	METEOSAT	Yes	<25.0 to >200.0	0.0–435.6	Used METEOSAT derived evapotranspiration in combination with 'mechanistic' formulations to compute biomass, no ground samples used	Rosema (1993)
Ferlo, Senegal (grassland)	1981 (n = 18, r = n/a)	Integrated AVHRR NDVI, empirical	No	<50.0–250.0	0.0–435.6	One of the first studies	Tucker et al. (1983)
All W.A. Sahel (all)	1981–1983 (n = 204, r = 0.83)	Integrated AVHRR NDVI, empirical	Yes	<35.0 to >175.0	0.0 to >600.0	Extrapolated NPP-NDVI model from 1980–1983 relationships developed for Ferlo, Senegal to all of W.A.	Tucker et al. (1985)
Niger (all)	1999 (n = n/a, r = n/a)	Integrated VEGETATION NDVI, empirical	Yes	<25.0 to >250.0	0.0 to >400	Used new VEGETATION sensor	Mougenot et al. (2000)

Of particular interest are those studies that have extended their estimates into the savannah zone where PAL GPP overestimated CENTURY GPP. For example, Diallo et al. (1991) mapped 1987–1988 above-ground NPP for Senegal (using an empirical model), whose southern portion extends into the savannah zone, and obtained values in excess of 500 g m^{-2}, in comparison to the current study, where values for this class exceeded 500 g m^{-2}, but rarely 600 g m^{-2}. Rasmussen's (1998) maps quantifying 1990–1991 above-ground NPP for Senegal show a similar range, as do Lo Seen Chong et al. (1993) for the upper portions of Nigeria. This boosts confidence in the values obtained for the savannah class with our LUE model.

8.4. LUE GPP versus integrated NDVI

The only conceivable, spatially exhaustive evaluation of our LUE model is to compare our GPP estimates against growing-season integrated NDVI. The integrated NDVI approach for estimating primary production was widely tested and applied in the 1980s and early 1990s (see Sections 3.1 and 3.2) for mapping NPP, but for lack of other information, we compare it with GPP. We summed NDVI values over the course of the growing season thereafter randomly sampling 1000 points from this image, as well as corresponding pixels from the GPP image (Fig. 4a). We then regressed integrated NDVI against GPP for three land cover classes, containing a sub-set of the sample points ($n = 283$ for grassland, $n = 255$ for savannah, and $n = 94$ for Cropland-vegetation Mosaic). Random sampling was implemented in order to avoid spatial autocorrelation effects (Burrough and McDonnell, 1998), while the purpose of the land cover stratification was to minimise heteroscedasticity in our regressions (Clark and Hosking, 1986) as well as to allow comparison of results between different vegetation

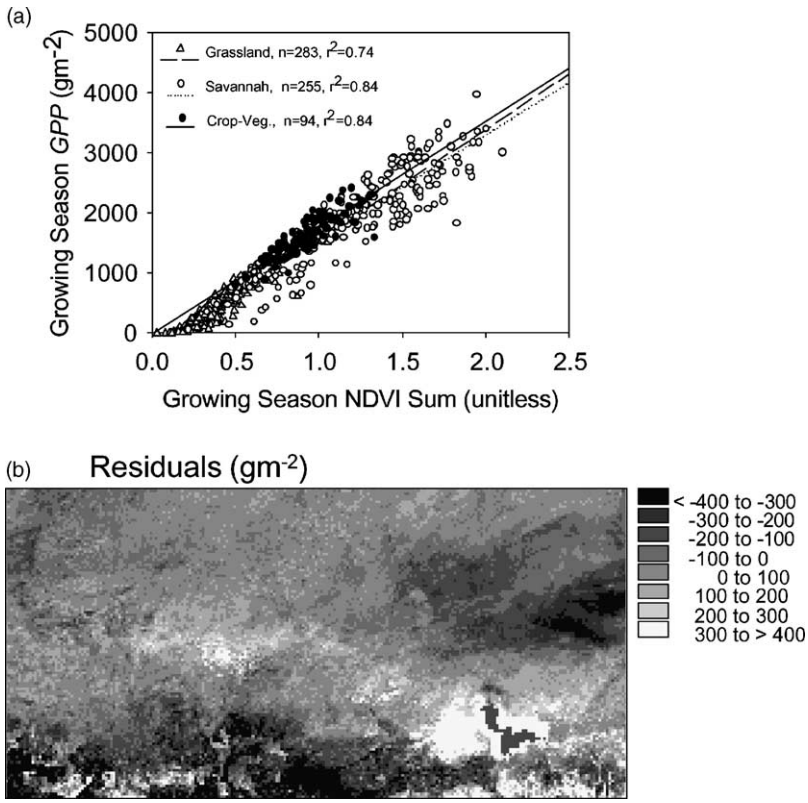

Fig. 7. (a) LUE-estimated GPP vs. integrated NDVI for three land cover classes based on random sampling. (b) Residuals of LUE-estimated GPP vs. integrated NDVI based on a random sample of 1000 pixels for entire region.

units. Fig. 7a shows that while the regressions between GPP and integrated NDVI for the three land cover classes are similar, a moderate amount of scatter is observed with r^2 values ranging from 0.74 (grassland) to 0.84 for the others. We then used the 1000 sampled points to regress growing season integrated NDVI against GPP for the entire region ($r^2 = 0.93$), thereafter using this equation to map the residuals from this regression in terms of GPP, shown in Fig. 7b. Despite the overall high correlation between the two images, relatively large differences are notable, especially in areas of greater biomass. In his 1998 paper, Rasmussen concluded that the spatial and temporal variation of the NPP-integrated NDVI relation stems from either variations in the biological growth efficiency, inconsistent response of the NDVI to environmental and climatic influences, or a combination of both. It follows that the unexplained variance in our GPP-integrated NDVI relation originates from the combined effects of ε (water stress scalar) and PAR, and in particular, the soil characteristics regulating transpiration. We do not explore Rasmussen's (1998) NDVI hypothesis in this paper.

9. Discussion and conclusions

There are a number of LUE-type models of varying complexity described in the literature, some of which use satellite data as a driver (e.g. Goetz et al., 1999), and others that are general enough to be applied to a number of different biomes including grasslands (e.g. Running and Hunt, 1993). Some of these models are designed for simulating the primary production in of forest stands (e.g. Landsberg and Waring, 1997) while most that use remotely-sensed data operate in the spatial domain. Yet others have been developed especially for semi-arid grasslands (Mougin et al., 1995). We have developed a model that yields estimates of grassland primary production as a map. Our model is similar to some of the others to the extent that it is embedded in a LUE framework. On a more detailed level, our approach is unique because it considers solely the water used by plants (actual transpiration) to index biological growth efficiency. This is particularly important for applications in partially vegetated landscapes where the fate of precipitation is highly controlled by relative amounts of vegetation. Our parameterisation of water stress is both pragmatic (given the data limitations) and biophysically realistic. This has been accomplished by subsuming classical and highly workable rangeland-yield formulations into our model (Eq. (3)). The combined use of the NDVI (Eqs. (4) and (5)), Ritchie's (1972) model of bare soil evaporation (Appendix D), as well as a bucket model (Eqs. (7)–(9)) facilitates this. After testing several other approaches for deriving spatially explicit fields of actual evapotranspiration (e.g. conventional bucket model where transpiration and bare soil evaporation are lumped together), this logic yields the most realistic and consistent results (see Fig. 3e). Since primary production in semi-arid rangelands is largely controlled by moisture limitations, this is an important part of our work.

Our model has merit because it has been developed for applications in data-impoverished parts of the world. These regions are often economically disadvantaged and undergoing a diminution of the natural resource base and are therefore in need of monitoring. Furthermore, recent evidence highlights the African Sahel as potentially important regulator of the tropical carbon budget. The sophisticated techniques that have become routine for accurately probing ecosystem processes in North America or Europe often cannot be supported over vast regions like the African Sahel. That we chose to develop our model for this area is motivated by such issues. We have therefore attempted to bridge gaps between data availability, representation of process, and model reliability, and spent some effort developing, and profiling how we actually derived the data layers in order to successfully apply our LUE model. Our methods exemplify a creative and efficient used sparse data set. Of particular significance is the use of the CLAVR layer from the PAL data set in order to derive, on a cell-by-cell basis, several important parameters pertaining to energy balance, including global and photosynthetically active radiation, net radiation, and potential evapotranspiration, among others. We have circumvented the need for using output from general circulation models, dense and extensive ground-based networks, or other data-intensive methods that rely on expensive or hard-to-get satellite data, and upon which other LUE models rely. Though ground data are lacking to provide a formal validation for these variables in the West African Sahel, indications are, based on mean monthly relative sunshine duration computed across the region

for available stations, little bias is incurred. However, we stress that the model could easily be applied in any grassland region where more conventional and accurate data sources exist. Recently, our model has been successfully applied, with slight modifications, to the rangelands of Inner Mongolia (Runnström et al., 2001; Brogaard et al., forthcoming). This is a testament to the general applicability and resiliency of our LUE model for other parts of the world.

Where possible, we have compared our derived variables with ground data, or performed sensitivity tests on various sub-models and components to ensure that our model performed in a robust manner. This was of major concern because formal validation is virtually impossible given the nature of the region for which we developed our model. Though all our evaluation exercises were informative, we believe that the results of the Monte Carlo simulations were particularly novel, striking, and useful. For example, it allowed us to identify where (geographically) our model is most likely to be unreliable—along the fringe of the northern fringe of the Sahel belt. To the best of our knowledge, no research as regards the spatial modelling of primary production has displayed results in such a manner. Additionally, not only were we able to identify those variables that contribute most to uncertainty in our maps, but we also showed that the contribution of error from any one particular variable varied across space, thus tipping the balance of error contribution from one variable to another from one sub-region to another.

This work is part of a larger, ongoing effort to quantify and explain carbon budget dynamics in the Sahel, a region where considerable knowledge gaps exist. Imminently, we are seeking to apply our LUE model to the full extent of the NOAA AVHRR archive in order quantify the inter-annual flow of carbon into the vegetation, and elucidate its uncertainties. Ultimately, we aim to elucidate the role that the Sahel plays in the tropical carbon budget.

Acknowledgements

This work was funded by the Swedish International Development Agency, and the Swedish National Space Board, while J.W. Seaquist was partly funded by Natural Sciences Engineering and Research Council of Canada. The Nordic-Africa Institute provided travel funds for J.W. Sseaquist. We are indebted to A. Warren, H. Osbahr, N. Taylor, and M. Seyni for assistance during the initial data gathering stages of this research. I.L. Mouhamadou of the Niger Meteorological Office in Niamey provided access to daily climate records. We thank A. Chappell and I. Clark for giving sound geostatistical advice. The help of M. Runnström for the temporal downscaling of rainfall is greatly appreciated. We also thank anonymous referees for comments that improved our manuscript. The satellite information that we used includes data produced through funding from the Earth Observing System Pathfinder Program of NASA's Mission to Planet Earth in cooperation with National Oceanic and Atmospheric Administration. The data were provided by the Earth Observing System Data and Information System (EOSDIS), Distributed Active Archive Center at Goddard Space Flight Center which archives, manages, and distributes this data set.

Appendix A

The algorithm necessary for obtaining solar irradiance at the top of the atmosphere (S_o) may be obtained from a number of different sources (e.g. Monteith and Unsworth, 1990; Shuttleworth, 1993; Haxeltine and Prentice, 1996). Each one varies in form depending how the parameters are lumped.

$$S_o = \frac{24(60)}{\pi} Q_o d_r (\omega_s \sin\phi \sin\delta + \cos\phi \cos\delta \sin\omega_s) \tag{A.1}$$

where S_o is the extraterrestrial irradiance (MJ m^{-2} day^{-1}), Q_o is the solar constant (0.0820 MJ m^{-2} min^{-1}), d_r is the relative Earth–Sun distance (unitless), ω_s is the sunset hour angle, ϕ is the latitude—positive in the northern hemisphere, negative in the southern (radians), and δ is the solar declination (radians).

The relative Earth–Sun distance, d_r, is:

$$d_r = 1 + 0.033 \cos\left(\frac{2\pi}{365} J\right) \tag{A.2}$$

where J is the Julian day number.

The sunset hour angle is given by:

$$\omega_s = \arccos(-\tan\phi \tan\delta) \tag{A.3}$$

The solar declination is, δ, is:

$$\delta = 0.4093 \sin\left(\frac{2\pi}{365} J - 1.405\right) \quad \text{(A.4)}$$

Ångström's formula for computing the amount of broad-band (global) radiation reaching the Earth's surface is:

$$S_t = S_o \left[a_s + b_s \left(\frac{n_i}{N}\right)\right] \quad \text{(A.5)}$$

where S_t is the solar radiation reaching the Earth's surface (MJ m^{-2} day^{-1}), S_o is the extraterrestrial irradiance (MJ m^{-2} day^{-1}), a_s is the fraction of global radiation S_o on overcast days, $a_s + b_s$ is the fraction global radiation reaching the Earth's surface on clear days, n_i is the sunshine duration (s), and N is the length of day (s).

The a_s and b_s terms were tailored to West African conditions after Davies (1966). n_i/N is given a value of 0 for CLAVR cells flagged as cloudy, while clear cells receive a value of 1. The mean value for the mixed cloud category, a priori unknown, was determined to be 0.4 based on calibration against ground observations of S_t from the HAPEX-Sahel experimental site (13°32′N and 2°39′E). Normalised root mean square errors of 15.69, 10.96, and 1.96% for 10-day, monthly, and yearly summation periods, respectively, were obtained (see Seaquist and Olsson, 1999 for details). Data on relative sunshine duration from nine stations scattered throughout Niger show that little spatial bias in incurred in estimated n_i/N (when compared to observed values) and hence S_t and PAR throughout the region. PAR is taken to be 48% of S_t.

Appendix B

The bracketed terms containing NDVI and raised to the exponent 2 in Eqs. (4) and (5) are fractional vegetation cover. NDVI is 're-normalised' which offers the following benefits: (1) numerical aesthetics; (2) insensitivity to viewing angle, sensor drift, and atmospheric contamination (Carlson et al., 1995). The term is then squared to obtain fractional vegetation cover (e.g. Choudhury et al., 1994; Carlson et al., 1995; Capehart, 1996; Carlson and Ripley, 1997). Ritchie (1972) expresses the energy available for phase 1 soil evaporation in terms of net radiation (R_n) and leaf area index (LAI). Replacing R_n with ET_p:

$$E_p = ET_p \exp(-c \times \text{LAI}) \quad \text{(B.1)}$$

where E_p is same as in Eq. (8) (bare soil evaporation) (mm), ET_p is same as in Eq. (6) (potential evapotranspiration) (mm), LAI is the Leaf Area Index, and c is the empirical parameter (unitless).

Following Choudhury et al. (1994) and Choudhury and DiGirolamo (1998), the fractional vegetation cover may be expressed as:

$$\text{Fr} = 1 - \exp(G \times \text{LAI}) \quad \text{(B.2)}$$

where Fr is the fractional vegetation cover (unitless), G is the value determined by leaf angle distribution.

Combining (D.1) and (D.2) yields:

$$E_p = ET_p(1 - \text{Fr})^{c/G} \quad \text{(B3)}$$

such that $c/G \approx 1$. This yields Eq. (8), and its inverse, Eq. (9). The derivation follows Choudhury and DiGirolamo (1998).

Appendix C

Net radiation is the sum net long-wave and net short-wave radiation (Shuttleworth, 1993):

$$R_n = S_t(1 - \alpha_s) - f\varepsilon' n\sigma(T + 273.2)^4 \quad \text{(C.1)}$$

where R_n is the net radiation (MJ m^{-2} day^{-1}), S_t is same as in Appendix A, α_s is the surface albedo (unitless), f is the adjustment for cloud cover (unitless), ε' is the net emissivity between the atmosphere and the ground (unitless), σ is the Stefan-Boltzmann constant (4.903×10^{-9} MJ m^{-2} K^{-4} day^{-1}), n is the number of days in the month, and T is the monthly mean air temperature (°C).

An adjustment for cloud cover, f, was determined as a by-product of the PAR (S_t) computation in Appendix A (Shuttleworth, 1993):

$$f = \left(a_c \frac{b_s}{a_s + b_s}\right)\frac{n_i}{N} + \left(b_c + \frac{a_s}{a_s + b_s} a_c\right) \quad \text{(C.2)}$$

where a_s is the constant as in Eq. (A.5), b_s is the constant as in Eq. (A.5), n_i is the sunshine duration as in Eq. (A.5), N is the day-length as in Eq. (A.5), $a_c = 1.35$, and $b_c = -0.35$.

The a_c and b_c coefficients are calibration parameters determined from measurements of long-wave radiation. For arid environments, the above values are recommended.

The net emissivity between the atmosphere and the ground was computed according to the following, as data for vapour pressure, dew point, and humidity were unavailable (Shuttleworth, 1993):

$$\varepsilon' = -0.02 + 0.261 \exp(-7.77 \times 10^{-4} T^{-2}) \quad \text{(C.3)}$$

where ε' is the net emissivity between the atmosphere and the land surface (unitless), and T is the monthly mean temperature in °C.

According to Song and Gao (1999) broad-band albedo may be recovered from the spectral-specific albedos by a linear combination of the RED and NIR channels of the NOAA AVHRR sensor:

$$\alpha_p = \beta_1 \text{RED} + \beta_2 \text{NIR} + \chi \quad \text{(C.4)}$$

where α_p is the planetary albedo (unitless), RED is the AVHRR channel 1 reflectance (unitless), NIR is the AVHRR channel 2 reflectance (unitless), β_1 is the empirically derived coefficient, β_2 is the empirically derived coefficient, and $\chi = 0$.

Both β_1 and β_2 are affected by vegetation amount, and are 'calibrated' by the NDVI:

$$\beta_1 = 0.494\text{NDVI}^2 - 0.329\text{NDVI} + 0.372 \quad \text{(C.5)}$$

$$\beta_2 = -1.439\text{NDVI}^2 + 1.209\text{NDVI} + 0.587 \quad \text{(C.6)}$$

Chen and Ohring (1984) empirically derived a solar zenith angle-dependent relation between planetary albedo derived from the NOAA AVHRR and surface albedo:

$$\alpha_p = a + b\alpha_s \quad \text{(C.7)}$$

where α_p is the planetary broad-band albedo, a is the constant depending on solar zenith angle, b is the constant depending on solar zenith angle, and α_s is the surface broad-band albedo.

The equation was re-arranged for α_s, and a look-up table given in Chen and Ohring (1984) was used to define a and b for solar zenith angle ranges. Chen and Ohring (1984) report root mean square errors of between 0.017 and 0.021 for solar zenith angles of 0 and 85°, respectively.

Appendix D

Before running the bucket model, we required an estimate of E_a (Eq. (7)), which we derived by applying the two-stage evaporation model of Ritchie (1972). Ritchie's model has been widely tested, especially at the plot scale (e.g. Wight and Hanks, 1981; Brutsaert and Chen, 1995; Wallace and Holwill, 1997; Wallace et al., 1999) but its application on regional or global scales is limited to Choudhury and DiGirolamo (1998).

In Ritchie's two-stage model, the first stage of bare soil evaporation occurs in the wake of a rainfall event, where soil evaporation is limited by the potential evaporation at the soil surface. This stage proceeds until the cumulative evaporation reaches a threshold (t_1) after which the de-sorption phase (stage 2) dominates. At this stage, the rate of evaporation depends on the square root of time and the hydraulic properties of the soil:

$$\sum E_{s1} = \sum_{i=0}^{t1} E_{pr} = U, \quad t < t_1 \quad \text{(D.1)}$$

$$\sum E_{s2} = k \times \sqrt{t - t_1}, \quad t > t_1 \quad \text{(D.2)}$$

$$E_a = \sum E_{s1} + \sum E_{s2} \quad \text{(D.3)}$$

where $\sum E_{s1}$ is stage 1 cumulative soil evaporation (mm), $\sum E_{s2}$ is stage 2 cumulative soil evaporation (mm), $\sum E_{so}$ is the potential evaporation for soil (mm), U is the total amount of water evaporated setting the upper limit for stage 1 evaporation (mm), k is the desorptivity mm day$^{-1/2}$, and E_a is the actual evaporation (mm).

In plot-based studies, the constants U and k are usually determined empirically (e.g. Ritchie, 1972) and depend on soil properties. They have been shown to range $k = 3.34$ ($U = 6$) for sandy soils to $k = 5.08$ ($U = 12$) for clay loams. According to Le Houerou (1980) the overwhelming majority of the soils in Niger are sandy, though black clayey soils (vertisols) may occur in local depressions. We therefore assigned values of $k = 3.5$ and $U = 6$, keeping in mind that soils throughout the region are composed mostly of sand with local occurrences of black clay. The k and U constants for sandy soils and black clays are very similar, based on the work of Ritchie (1972) and Black et al. (1969). Unlike Ritchie's original model, we ignored the impact of shading (acting to suppress vapour pressure deficit and wind speed) as this had an insignificant impact on our final results.

Appendix E

An important prerequisite for the use of Ritchie's (1972) model for bare soil evaporation is that daily rainfall records are available. The statistical downscaling of rainfall from monthly to daily values is not trivial, especially for spatially distributed rainfall fields. Weather generators can achieve this (e.g. Jones and Thornton, 1997; Friend, 1998). We adopted a simpler approach. We inspected cumulative monthly frequency histograms of daily rainfall data for 15 stations across Niger. For most stations during the rainy season (defined here as May–October), over 50% of the rainfall that fell in each month occurred in short, intense bursts, between one and three times (rounded off to the nearest whole number). The low magnitude events comprised the lower 5% of the rainfall totals and occurred between two and five times. The remaining 45% of the rainfall occurred between two and six times. Accordingly, the interpolated monthly total rainfall surfaces were divided into three categories, comprising 5, 45 and 50% of the monthly totals. Rainfall events were treated as a time-dependent random process (using a random number generator in FORTRAN), and no restrictions were made as regards the number of rainfall events of a given magnitude occurring within a cell on a given pseudo-day. Re-aggregation of the daily rainfall for the entire area to monthly totals faithfully reproduced the monthly rainfall surfaces and verified the consistency of our method.

Appendix F

We tested the impact on computed E_a aggregated over a 37-day period by artificially partitioning daily rainfall as in Appendix D with the rainfall and E_a data set provided by Ritchie (1972). Use of the actual rainfall series produced a total E_a of 60.6 mm, whereas the simulated rainfall series gave 57.4 mm, an underestimation of 5.3%.

References

Africa Data Dissemination Service (ADDS) of the USGS, http://edcsnw4.cr.usgs.gov/adds/adds.html.

Agnew, C.T., Chappell, A., 1999. Drought in the Sahel. GeoJournal 70, 299–311.

Ångström, A., 1924. Solar and terrestrial radiation. Q. J. R. Met. Soc. 50, 121–126.

Ardö, J., Olsson, L., 2002. Assessment of soil organic carbon in semi-arid Sudan using GIS and the CENTURY model. J. Arid Env. 54, 633–651.

Bartholome, E., 1990. Estimation of APAR values from AVHRR NDVI for regional crop yield assessment in West Africa. In: Proceedings of IGARSS'90 Symposium Technologies for the Nineties, Washington, DC, May 21–24, 1990, pp. 587–590.

Bastiaanssen, W.G.M., 1995. Regionalization of Surface Flux Densities and Moisture Indicators in Composite Terrain—A Remote Sensing Approach Under Clear Skies in Mediterranean Climates. Ph.D. Thesis, Winand Staring Centre, Wageningen, The Netherlands, 273 pp.

Begue, A., 1993. Leaf area index, intercepted photosynthetically active radiation, and spectral vegetation indices: a sensitivity analysis for regular-clumped canopies. Rem. Sens. Env. 46, 45–59.

Begue, A., Desprat, J.F., Imbernon, J., Baret, F., 1991. Radiation use efficiency of pearl millet in the Sahelian zone. Agric. For. Met. 56, 93–110.

Black, T.A., Gardner, W.R., Thurtell, G.W., 1969. The prediction of evaporation, drainage, and soil water storage for a bare soil. Soil Sci. Soc. Am. Proc. 33, 655–660.

Box, E.O., Holben, B.N., Kalb, V., 1989. Accuracy of the AVHRR Vegetation Index as a predictor of biomass, primary productivity, and net CO_2 flux. Vegetatio 80, 71–89.

Brogaard, S., Runnström, M., Seaquist, J.W., forthcoming. Primary production of Inner Mongolia, China, between 1982 and 1999 estimated by a satellite data-driven light use efficiency model. Submitted for publication.

Bromberg, J.G., McKeown, R., Knapp, L., Kittel, T.G.F., Ojima, D.S., 1996. Integrating GIS and the CENTURY model to manage and analyse data. GIS and Environmental Modeling: Progress and Research Issues 429–431.

Brutsaert, W., Chen, D., 1995. Desorption and the two stages of drying of natural tallgrass prairie. Water Resour. Res. 31, 1305–1313.

Burke, I.C., Yonker, C.M., Cole, C.V., Flach, K., Schimel, D.S., 1989. Texture, climate, and cultivation effects on soil organic matter context in U.S. grassland soils. Soil Sci. Soc. Am. J. 53, 800–805.

Burrough, P.A., McDonnell, R.A., 1998. Principles of Geographic Information Systems. Oxford University Press, 333 pp.

Capehart, W.J., 1996. Issues Regarding the Remote Sensing and Modeling of Soil Moisture for Meteorological Applications. Ph.D. Thesis, Earth Systems Science Center, Pennsylvania State University, 238 pp.

Carlson, T.N., Ripley, D.A., 1997. On the relation between NDVI, fractional vegetation cover, and leaf area index. Rem. Sens. Env. 62, 241–252.

Carlson, T.N., Capehart, W.J., Gillies, R.R., 1995. A new look at the simplified method for remote sensing of daily evapotranspiration. Rem. Sens. Env. 54, 161–167.

CESBIO, ORSTOM, CNES, 1997. HAPEX-Sahel Information System, http://www.ird.fr/hapex/.

Chappell, A., Seaquist, J.W., Eklundh, L., 2001. Improving the estimation of noise from NOAA AVHRR NDVI for Africa using geostatistics. Int. J. Rem. Sens. 22, 1067–1080.

Chen, T.S., Ohring, G., 1984. On the relationship between clear-sky planetary and surface albedo. J. Atmos. Sci. 41, 156–158.

Cherchali, S., Amram, O., Flouzat, G., 1995. The improvement of net primary productivity estimation taking into account the heterogeneity of Sahelian region. In: Proceedings of IGARSS'95, Firenze, Italy, July 12–14, 1995, pp. 1230–1233.

Choudhury, B.J., 1994. Synergism of multispectral satellite observations for estimating regional land surface evaporation. Rem. Sens. Env. 49, 264–274.

Choudhury, B.J., DiGirolamo, N.E., 1998. A biophysical process-based estimate of global land surface evaporation using satellite and ancillary data. I. Model description and comparison with observations. J. Hydrol. 205, 164–185.

Choudhury, B.J., Ahmed, N.U., Idso, S.B., Reginato, R.J., Daughtry, C.S.T., 1994. Relations between evaporation coefficients and vegetation indices studied by model simulations. Rem. Sens. Env. 50, 1–17.

Clark, W.A.V., Hosking, P.L., 1986. Statistical Methods for Geographers. Wiley, 518 pp.

Cole, C.V., Stewart, J.W.B., Ojima, D.S., Parton, W.J., Schimel, D.S., 1989. Modelling land use effects of soil organic matter dynamics in the North American Great Plains. In: Clarholm, M., Bergström, L. (Eds.), Ecology of Arable Land. Kluwer Academic Publishers, Amsterdam, The Netherlands, pp. 89–98.

Coops, N.C., Waring, R.H., Brown, S.R., Running, S.W., 2001. Comparisons of predictions of net primary production and seasonal patterns in water use derived with two forest growth models in Southwestern Oregon. Ecol. Model. 142, 61–81.

Crosetto, M., Ruis, J.A.M., Crippa, B., 2001. Uncertainty propagation in models driven by remotely sensed data. Rem. Sens. Env. 76, 373–385.

Davies, J.A., 1966. The assessment of evapotranspiration for Nigeria. Geogr. Ann. 48A, 139–166.

Diallo, O., Diouf, A., Hanan, N.P., Ndiaye, A., Prevost, Y., 1991. AVHRR monitoring of savannah primary production in Senegal, West Africa: 1987–1988. Int. J. Rem. Sens. 12, 1259–1280.

Eklundh, L., 1996. AVHRR NDVI for Monitoring and Mapping of Vegetation and Drought in East African Environments. Meddelanden från Lunds Universitets Geografiska Institutioner, Avhandlingar, pp. 126, 187.

Eklundh, L., Olsson, L., 2003. Vegetation index trends for the African Sahel 1982–1999. Geophys. Res. Lett. 30, 1430, doi:10.1029/2002GL016772.

FAO/UNESCO, 1995. Digital Soil Map of the World and Derived Properties Version 3.5. Food and Agriculture Organization of the United Nations.

Field, C.B., Randerson, J.T., Malmström, C.M., 1995. Global net primary production: combining ecology and remote sensing. Rem. Sens. Env. 51, 74–88.

Friend, A.D., 1998. Parameterisation of a global daily weather generator for terrestrial ecosystem modelling. Ecol. Model. 109, 121–140.

Frouin, R., Pinker, R.T., 1995. Estimating photosynthetically active radiation (PAR) at the Earth's surface from satellite observations. Rem. Sens. Env. 51, 98–107.

Goetz, S.J., Prince, S.D., 1999. Modelling terrestrial carbon exchange and storage: evidence and implications of functional convergence light use efficiency. Adv. Ecol. Res. 28, 57–92.

Goetz, S.J., Prince, S.D., Goward, S.N., Thawley, M.M., Small, J., 1999. Satellite remote sensing of primary production: an improved production efficiency modeling approach. Ecol. Model. 122, 239–255.

Goovaerts, P., 1997. Geostatistics for Natural Resource Evaluation. Oxford University Press, 483 pp.

Goward, S.M., Huemmrich, K.E., 1992. Vegetation canopy PAR absorptance and the Normalized Difference Vegetation Index: an assessment using the SAIL model. Rem. Sens. Env. 39, 119–140.

Gower, S.T., Kucharik, C.J., Norman, J.M., 1999. Direct and indirect estimation of leaf area index, FAPAR, and net primary production of terrestrial ecosystems. Rem. Sens. Env. 70, 29–51.

Guerif, M., de Brisis, S., Seguin, B., 1993. Combined NOAA-AVHRR and SPOT-HRV data for assessing crop yields of semi-arid environments. EARSeL Adv. Rem. Sens. 2, 110–123.

Hall, D.O., Rao, K.K., 1994. Photosynthesis. Cambridge University Press, 211 pp.

Hanan, N.P., Prince, S.D., Begue, A., 1995. Estimation of absorbed photosynthetically active radiation and vegetation net production efficiency using satellite data. Agric. For. Met. 76, 259–276.

Hanan, N.P., Prince, S.D., Begue, A., 1997. Modelling vegetation primary production during HAPEX-Sahel using production efficiency and canopy conductance model formulations. J. Hydrol. 188/189, 651–675.

Handcock, R., 2001. Spatio-Temporal Analysis of Net Primary Production Across Ontario Using an Ecoregionalization. Ph.D. Thesis, University of Toronto, Toronto, Ont., Canada, 150 pp.

Hanks, R.J., 1974. Model for predicting plant yield as influenced use. Agron. J. 66, 660–665.

Haxeltine, A., Prentice, I.C., 1996. BIOME3: an equilibrium terrestrial biosphere model based on ecophysiological constraints, resource availability, and competition among plant functional types. Glob. Biogeochem. Cycles 10, 693–709.

Heuvelink, G.B.M., 1998. Error Propagation in Environmental Modelling with GIS. Taylor & Francis, London, 127 pp.

Holben, B.N., 1986. Characteristics of maximum-value composite images from temporal AVHRR data. Int. J. Rem. Sens. 7, 1417–1437.

Hulme, M., 1989. Is environmental degradation causing drought in the Sahel? An assessment from recent empirical research. Geography 38–46.

Hunt Jr., E.R., 1994. Relationship between woody biomass and PAR conversion efficiency for estimating net primary production from NDVI. Int. J. Rem. Sens. 15, 1725–1730.

James, M.E., Kalluri, S.N.V., 1994. The Pathfinder AVHRR land data set: an improved coarse resolution data set for terrestrial monitoring. Int. J. Rem. Sens. 15, 3347–3363.

Jensen, R.E., Burman, R.D., Allen, R.G., 1990. Evapotranspiration and irrigation water requirements. ASCE Manual 70, 332.

Jiang, L., Islam, S., 1999. A methodology for estimation of surface evapotranspiration over large areas using remote sensing observations. Geophys. Res. Lett. 26, 2773–2776.

Jones, P.G., Thornton, P.K., 1997. Spatial and temporal variability of rainfall related to a third-order Markov model. Agric. For. Met. 86, 127–138.

Justice, C.O., Hiernaux, P.H.Y., 1986. Monitoring the grasslands of the Sahel using NOAA AVHRR data: Niger 1983. Int. J. Rem. Sens. 7, 1515–1532.

Kaisischke, E.S., French, N.H.F., 1997. Constraints on using AVHRR composite index imagery to study patterns of vegetation cover in boreal forest. Int. J. Rem. Sens. 18, 2403–2426.

Kaufman, Y.J., Tanre, D., 1996. Strategy for direct and indirect methods for correcting the aerosol effect on remote sensing: from AVHRR to EOS-MODIS. Rem. Sens. Env. 55, 65–79.

Kimball, J.S., White, M.A., Running, S.W., 1997. BIOME-BGC simulations of stand hydrologic processes for BOREAS. J. Geophys. Res. 102 (D24), 29043–29051.

L'homme, J.-P., 1996. A theoretical basis for the Priestley-Taylor coefficient. Boundary Layer Met. 82, 179–191.

Landsberg, J.J., Waring, R.H., 1997. A generalised model of forest productivity using simplified concepts of radiation-use efficiency, carbon balance and partitioning. For. Ecol. Manage. 95, 209–228.

Le Houerou, H.N., 1980. The rangelands of the Sahel. J. Range Manage. 33, 41–46.

Le Houerou, H.N., Popov, G.F., See, L., 1993. Agro-Bioclimatic Classification of Africa. Working Paper Number 6, FAO Meteorology Series.

Lind, M., Fensholt, R., 1999. The spatio-temporal relationship between rainfall and vegetation development in Burkina Faso. Danish J. Geog. (Special Issue 2), 43–55.

Lobell, D.B., Hicke, J.A., Asner, G.P., Field, C.B., Tucker, C.J., Los, S.O., 2002. Satellite estimates of productivity and light use efficiency in United States agriculture, 1982–1998. Glob. Chem. Biol. 8, 722–735.

Lo Seen Chong, D., Mougin, E., Gastellu-Etchegorry, J.P., 1993. Relating the Global Vegetation Index to net primary productivity and actual evapotranspiration over Africa. Int. J. Rem. Sens. 14, 1517–1546.

Loveland, T.R., Zhu, Z., Ohlen, D.O., Brown, J.F., Reed, B.C., Yang, L., 1999. An analysis of the IGBP global land-cover characterization process. Photogr. Eng. Rem. Sens. 65, 1021–1032.

Maisongrande, P., Ruimy, A., Dedieu, G., Saugier, B., 1995. Monitoring seasonal and interannual variations of gross primary productivity, net primary productivity and net ecosystem productivity using a diagnostic model and remotely-sensed data. Tellus 47B, 178–190.

Maselli, F., Conese, C., Petkov, L., Gilabert, M.A., 1992. Use of NOAA-AVHRR NDVI data for environmental monitoring and crop forecasting in the Sahel. Preliminary results. Int. J. Rem. Sens. 14, 2743–2749.

Matheron, M.A., 1971. The Theory of Regionalized Variables and Its Applications, vol. 5. Centre de Morpholgie Mathematique de Fountainbleau, Fountainebleau.

Metherell, A.K., Harding, L.A., Cole, C.V., Parton, W.J., 1993. CENTURY Soil Organic Matter Environment, Technical Documentation, Agroecosystem Version 4.0. United States Department of Agriculture, Agricultural Research Service, Great Plaines System Research Unit. Technical Report #4.

Mikhailova, E.A., Bryant, R.B., DeGloria, S.D., Post, C.J., Vessenev, I.I., 2000. Modeling soil organic matter dynamics after conversion of native grassland to long-term continuous fallow using the CENTURY model. Ecol. Model. 132, 247–257.

Millington, A.C., Wellens, J., Settle, J.J., Saull, R.J., 1994. Explaining and monitoring land cover dynamics in drylands using multitemporal analysis of NOAA AVHRR imagery. In: Foody, G., Curran, P. (Eds.), Environmental Remote Sensing from Regional to Global Scales. Wiley, Chechester, pp. 16–43.

Monteith, J.L., 1972. Solar radiation and productivity in tropical ecosystems. J. Appl. Ecol. 9, 747–766.

Monteith, J.L., 1977. Climate and the efficiency of crop production in Britain. Phil. Trans. R. Soc. Lond. 281, 277–294.

Monteith, J.L., Unsworth, M., 1990. Principles of Environmental Physics. Arnold, London, 291 pp.

Mougenot, B., Begue, A., Chehbouni, G., Escadafal, R., Heilman, P., Qi, J., Royer, A., Watts, C., 2000. Applications of VEGETATION Data to Resource Management in Arid and Semi-Arid Rangelands. 7 pp.

Mougin, E., Lo Seen, D., Rambal, S., Gaston, A., Hiernaux, P., 1995. A regional Sahelian grassland model to be coupled with multispectral satellite data. I. Model description and validation. Rem. Sens. Env. 52, 181–193.

Myneni, R.B., Williams, D.L., 1994. On the relationship between FAPAR and NDVI. Rem. Sens. Env. 49, 200–211.

Nicholson, S.E., Lare, A.R., Marengo, J.A., Santos, P., 1996. A revised version of Lettau's evapoclimatonomy model. J. Appl. Met. 35, 549–561.

Nicholson, S.E., Tucker, C.J., Ba, M.B., 1998. Desertification, drought, and surface vegetation: an example from the West African Sahel. Bull. Am. Met. Soc. 79, 815–829.

Olsson, L., 1993. Desertification in Africa—a critique and an alternative approach. GeoJournal 31, 23–31.

Parton, W.J., Schimel, D.S., Cole, C.V., Ojima, D.S., 1987. Analysis of factors controlling soil organic levels of grasslands in the Great Plains. Soil Sci. Soc. Am. J. 51, 1173–1179.

Parton, W.J., Stewart, J.W.B., Cole, C.V., 1988. Dynamics of C, N, P, and S in grassland soils: a model. Biogeochemistry 5, 109–131.

Parton, W.J., Scurlock, J.M.O., Ojima, D.S., Gilmanov, T.G., Scholes, R.J., Schimel, D.S., Kirchner, T., Menaut, J.-C., Seastedt, T., Moya, E.G., et al., 1993. Observations and modelling of biomass and soil organic matter dynamics for the grassland biome worldwide. Glob. Biogeochem. Cycles 7, 785–809.

Parton, W.J., Ojima, D.S., Schimel, D.S., 1994. Environmental change in grasslands: assessment using models. Clim. Change 28, 111–114.

Parton, W.J., Coughenour, M.B., Scurlock, J.M.O., Ojima, D.S., Gilmanov, T.G., Scholes, R.J., Schimel, D.S., Kirchner, T.B., Menaut, J.-C., Seastedt, T.R., et al. 1996. Global grassland ecosystem modelling: development and test of ecosystem models for grassland ecosystems. In: Breymeyer, A.I., Hall, D.O., Mellilo, J.M., Ågren, G.I. (Eds.), Global Change: Effects on Coniferous Forests and Grasslands. Wiley, New York, pp. 229–279.

Potter, C.S., Randerson, J.T., Field, C.B., Matson, P.A., Vitousek, P.M., Mooney, H.A., Klooster, S.A., 1993. Terrestrial ecosystem production: a process model based on global satellite and surface data. Glob. Biogeochem. Cycles 7, 811–841.

Priestley, C.H.B., Taylor, R.J., 1972. On the assessment of surface heat flux and evaporation using large-scale parameters. Monthly Weather Rev. 100, 81–92.

Prince, S.D., 1991a. Satellite remote sensing of primary production: comparison of results for Sahelian grasslands 1981–1988. Int. J. Rem. Sens. 12, 1301–1312.

Prince, S.D., 1991b. A model of regional primary production for use with coarse resolution satellite data. Int. J. Rem. Sens. 12, 1313–1330.

Prince, S.D., Goward, S.N., 1995. Global primary production: a remote sensing approach. J. Biogeogr. 22, 815–835.

Prince, S.D., Kerr, Y.H., Goutorbe, J.-P., Lebel, T., Tinga, A., Bessemoulin, P., Brouwer, J., Dolman, A.J., Engman, E.T., Gash, J.H.C., Hoepffner, M., Kabat, P., Monteny, B., Said, F., Sellers, P., 1995. Geographical, biological, and remote sensing aspects of the hydrologic atmospheric pilot experiment in the Sahel (HAPEX-Sahel). Rem. Sens. Env. 51, 215–234.

Prince, S.D., Brown de Coulstoun, E., Kravitz, L.L., 1998. Evidence from rain-use efficiencies does not indicate extensive Sahelian desertification. Glob. Change. Biol. 4, 359–374.

Rasmussen, M.S., 1998. Developing simple, operational, consistent NDVI-vegetation models by applying environmental and climatic information. Part I. Assessment of net primary production. Int. J. Rem. Sens. 19, 97–117.

Ruimy, A., Dedieu, G., Saugier, B., 1996. TURC: a diagnostic model of continental gross primary productivity and net primary productivity. Glob. Biogeochem. Cycles 10, 269–286.

Reeves, M.C., Winslow, J.C., Running, S.W., 2001. Mapping weekly rangeland vegetation productivity using MODIS algorithms. J. Range Manage. 54, 90–105.

Ritchie, J.T., 1972. Model for predicting evaporation from a row crop with incomplete cover. Water Resour. Res. 8, 1204–1213.

Rockström, J., 1997. On-Farm Agrohydrological Analysis of the Sahelian Yield Crisis: Rainfall Partitioning, Soil Nutrients, and Water Use Efficiency of Pearl Millet. Akademitryck AB, Stockholm.

Rosema, A., 1993. Using METEOSAT for operational evapotranspiration and biomass monitoring in the Sahel region. Rem. Sens. Env. 46, 27–44.

Ruimy, A., Dedieu, G., Saugier, B., 1996. TURC—Terrestrial Uptake and Release of Carbon by vegetation: a diagnostic model of continental gross primary productivity and net primary productivity. Glob. Biogeochem. Cycles 10, 269–285.

Running, S.W., Hunt Jr., E.R., 1993. Generalization of a forest ecosystem process model for other biomes, BIOME-BGC, and an application for global-scale models. In: Ehleringer, J.R., Field, C. (Eds.), Scaling Processes Between Leaf and Landscape Levels. Academic Press, pp. 141–158.

Runnström, R., Brogaard, S., Seaquist, J.W., 2001. A satellite data-driven parametric model of primary production implemented over the inner Mongolian rangeland of northern China. In: Challenges of a Changing Earth: A Global Change Open Science Conference, Amsterdam, July 10–13, 2001 (Category: Sustaining the Land: Food, Biodiversity, and Other Services).

Runyon, J., Waring, R.H., Goward, S.N., Welles, J.M., 1994. Environmental limits on net primary production and light-use efficiency across the Oregon transect. Ecol. Appl. 4, 226–237.

Schimel, D.S., et al., 2001. Recent patterns and mechanisms of carbon exchange by terrestrial ecosystems. Nature 414, 169–172.

Seaquist, J.W., 2001. Mapping Primary Production for the West African Sahel with Satellite Data. Ph.D. Thesis, Meddelanden fran Lunds Universitets Geografiska Institutioner, Avhandlingar, pp. 140, 198.

Seaquist, J.W., Olsson, L., 1999. Rapid estimation of photosynthetically active radiation over the West African Sahel using the Pathfinder Land Data Set. Int. J. Earth Obs. Geoinf. 1, 205–213.

Shuttleworth, W.J., 1993. Evaporation. In: Maidment, D.R. (Ed.), Handbook of Hydrology. McGraw-Hill, New York.

Smith, P.M., Kalluri, S.N.V., Prince, S.D., DeFries, R., 1997a. The NOAA/NASA Pathfinder AVHRR 8-km Land Data Set. Photogram. Eng. Rem. Sens. LXIII, 12–32.

Smith, P., Smith, J.U., Powlson, D.S., McGill, W.B., Arah, J.R.M., Chertov, O.G., Coleman, K., Frankoe, U., Frolkning, S., Jenkinson, D.S., et al., 1997b. A comparison of the performance of nine soil organic matter models using data sets from seven long-term experiments. Geoderma 81, 153–225.

Song, J., Gao, W., 1999. An improved method to derive surface albedo from narrowband AVHRR satellite data: narrowband to broadband conversion. J. Appl. Met. 38, 239–249.

Soufflet, V., Tanre, D., Begue, A., Podaire, A., Deschamps, P.Y., 1991. Atmospheric effects on NOAA/AVHRR imagery over Sahelian regions. Int. J. Rem. Sens. 12, 1189–1203.

Srivastava, S.K., Jayaraman, V., Nageswara Rao, P.P., Manikiam, B., Chandrasekhar, M.G., 1997. Interlinkages of NOAA/AVHRR derived integrated NDVI to seasonal precipitation and transpiration in dryland tropics. Int. J. Rem. Sens. 18, 2931–2952.

Tucker, C.J., Vanpraet, C., Boerwinkel, E., Gaston, A., 1983. Satellite remote sensing of total dry matter production in the Senegalese Sahel. Rem. Sens. Env. 13, 461–474.

Tucker, C.J., Vanpraet, C.L., Sharman, M.J., van Ittersum, G., 1985. Satellite remote sensing of total herbaceous biomass production in the Senegalese Sahel: 1980–1984. Rem. Sens. Env. 17, 233–250.

USGS EROS Data Center Distributed Archive Center, 2000. Africa Land Cover Characteristics Data Base Version 1.2 at http://edcdaac.usgs.gov/glcc/tabgoode_af.html.

Veroustraete, F., Patyn, J., Myneni, R.B., 1996. Estimating net ecosystem exchange of carbon using the normalized difference vegetation index and an ecosystem model. Rem. Sens. Env. 58, 115–130.

Verstraete, M.M., Pinty, B., 1991. The potential contribution of satellite remote sensing to the understanding of arid lands processes. Vegetatio 91, 59–72.

Viovy, N., Arino, O., Belward, A.S., 1992. The best index slope extraction (BISE): a method for reducing noise in NDVI time-series. Int. J. Rem. Sens. 13, 1585–1590.

Vose, R.S., Schmoyer, R.L., Steurer, P.M., Peterson, T.C., Heim, R., Karl, T.R., Eischeid, J.K., 1992. The global historical climatology network: long-term monthly temperature, precipitation, sea level pressure, and station pressure data version 2.0, http://cdiac.esd.ornl.gov/epubs/ndp/ndp041/ndp041.html.

Wallace, J.S., Holwill, C.J., 1997. Soil evaporation from tiger-bush in south-west Niger. J. Hydrol. 188/189, 426–442.

Wallace, J.S., Lloyd, C.R., Sivakumar, M.V.K., 1993. Measurements of soil, plant, and total evaporation from millet in Niger. Agric. For. Met. 63, 149–169.

Wallace, J.S., Jackson, N.A., Ong, C.K., 1999. Modelling soil evaporation in an agroforestry system in Kenya. Agric. For. Met. 94, 189–202.

White, J.D., Running, S.W., 1994. Testing scale dependent assumptions in regional ecosystem simulations. J. Veg. Sci. 5, 687–702.

Wight, J.R., Hanks, R.J., 1981. A water-balance, climate model for range herbage production. J. Range Manage. 34, 307–311.

Wylie, B.K., Harrington, J.A., Prince, S.D., Denda, I., 1991. Satellite and ground-based pasture production assessment in Niger: 1986–1988. Int. J. Rem. Sens. 12, 1281–1300.

Wythers, K.R., Laurenroth, W.K., Paruelo, J.M., 1999. Bare-soil evaporation under semiarid field conditions. Soil Sci. Am. J. 63, 1341–1349.